OpenNano 21 (2025) 100228

Contents lists available at ScienceDirect

OpenNano

journal homepage: www.elsevier.com/locate/onano

Chitosan-Coated silver nanoparticles with various floral honey bioreductors: A promising nonalcoholic hand gel sanitizer formulation

Saidun Fiddaroini [a], Kurnia Indu [a], Luailik Madaniyah [a], Suci Amalia [b], Aulanni'am [a], Moh. Farid Rahman [a], Akhmad Sabarudin [a,c,*]

[a] Department of Chemistry, Faculty of Science, Brawijaya University, Malang, Indonesia
[b] Chemistry Study Program, Faculty of Science and Technology, Maulana Malik Ibrahim Islamic State University, Malang, Indonesia
[c] Research Center for Advanced System and Material Technology, Brawijaya University, Malang, Indonesia

ARTICLE INFO

Keywords:
Silver nanoparticles
Honey
Chitosan
Antibacterial
Hand gel sanitizer

ABSTRACT

Antimicrobial resistance represents a critical global health challenge, necessitating innovative strategies to combat resistant pathogens. In this study, silver nanoparticles (AgNPs) were synthesized using honey as a bioreductant and coated with oligochitosan derived from the depolymerization of low-molecular-weight chitosan. The synthesis employed eco-friendly methods, with characterization performed via UV–Vis spectroscopy, FTIR, TEM, EDX, XRD, and LC—HRMS. AgNPs synthesized with *Ceiba pentandra* honey exhibited an average particle size of 11.71 nm, demonstrating high antibacterial activity when coated with oligochitosan. The 10 % AgNPs-Chitosan-based hand gel sanitizer formulation achieved inhibition zones of 14.84 ± 0.40 mm against *Staphylococcus aureus* and 11.16 ± 0.73 mm against *Pseudomonas aeruginosa.* The hand gel sanitizer formulation exhibited stable pH (4.0–4.3), high resistance to syneresis at 5 °C and 40 °C, and superior antibacterial efficacy compared to alcohol-based hand gel sanitizers. Dermatological assessments confirmed the formulation's safety, and *Artemia salina* toxicity tests revealed the highest LC_{50} value (2,648.97 ppm) for AgNPs derived from *C. pentandra* honey. This work provides an eco-friendly, efficient method for AgNP synthesis with strong potential for biomedical and environmental applications, including their use in hand gel sanitizers to reduce pathogen transmission in various settings, contributing to the advancement of green nanotechnology.

1. Introduction

Antimicrobial resistance (AMR) refers to the capacity of microorganisms, such as bacteria and viruses, to resist the effects of drugs designed to eliminate or inhibit them, rendering treatments ineffective [1]. This global health threat poses significant challenges, particularly as AMR-related infections are projected to cause up to 10 million deaths annually by 2050 if left unchecked [2]. Overuse

Abbreviations: EDX, Energy-dispersive X-ray; GML, Gell mass loss; GM, Gell mass; LMW, Low-molecular-weight; NA, Nutrient agar; TEM, Transmission electron microscopy; XRD, X-ray diffraction; FTIR, Fourier Transform Infra-red; AgNPs, Silver Nanoparticles; AgNPs-Chitosan, Chitosan-coated Silver Nanoparticle; ZP, Zeta Potential.

* Corresponding author.
E-mail address: sabarjpn@ub.ac.id (A. Sabarudin).

https://doi.org/10.1016/j.onano.2024.100228
Received 22 October 2024; Received in revised form 22 December 2024; Accepted 27 December 2024
Available online 27 December 2024

and misuse of antibiotics are the primary drivers of this phenomenon, accelerating genetic mutations in microorganisms that enable resistance [3,4]. Consequently, there is a pressing need to develop alternative strategies to combat resistant pathogens and mitigate the risks posed by AMR.

Metal nanoparticles, particularly AgNPs, have emerged as promising candidates in combating pathogenic bacteria [5]. AgNPs are highly effective due to their small size (less than 100 nm), which increases their surface area-to-volume ratio and enhances their antimicrobial activity [6,7]. These nanoparticles disrupt bacterial membranes, penetrate cells, and induce toxicity through oxidative stress and DNA damage [8–10]. Moreover, AgNPs demonstrate significant antibiofilm activity, providing an edge over conventional antibiotics [11–13]. The ability to harness AgNPs as antimicrobial agents underscores the importance of sustainable synthesis methods that optimize their properties while minimizing environmental and health risks.

AgNPs can be synthesized through physical, chemical, or biological methods, with biological synthesis gaining attention for its eco-friendly approach [14–18]. Honey, a natural bioreductor, is particularly advantageous for AgNP synthesis due to its ability to produce uniformly small nanoparticles with enhanced antibacterial properties [19–21]. Additionally, chitosan, a biodegradable biopolymer, has been widely studied as a capping and stabilizing agent for AgNPs [22]. Chitosan not only prevents nanoparticle agglomeration but also enhances antimicrobial activity through controlled silver ion release and its intrinsic antibacterial properties [23–26]. The Zeta potential analysis showed that the AgNPs-chitosan exhibited a higher stability with a ZP value of −28.08, compared to the uncoated AgNPs, which showed a ZP value of −24.51. This indicates that the chitosan coating significantly improves the colloidal stability and reduces agglomeration, as higher negative Zeta potential values are associated with better stability and less particle aggregation [27]. Despite the promising potential of honey and chitosan, the variability in honey's chemical composition, influenced by factors like plant origin and location [28,29], necessitates further exploration to optimize their combined use in AgNP synthesis.

Hand gel sanitizers represent a practical application for AgNPs, particularly as antibacterial agents in non-alcoholic formulations [30]. Traditional alcohol-based sanitizers, while effective, can cause skin irritation with frequent use [31]. Chitosan-coated AgNPs (AgNPs-Chitosan), derived from honey-based synthesis, offer a safer alternative with strong antimicrobial efficacy and minimal skin damage [20,32,33]. Gel-based hand gel sanitizers, in particular, benefit from the incorporation of AgNPs due to their prolonged retention on the skin and enhanced antibacterial activity [34,35]. By leveraging the synergistic effects of honey and chitosan, it is possible to develop sustainable, non-alcoholic hand gel sanitizers with high efficacy against both Gram-positive and Gram-negative bacteria.

This study aims to synthesize AgNPs using honey-based reducing agents and subsequently coat them with oligochitosan derived from the depolymerization of low molecular weight (LMW) chitosan. The AgNPs-Chitosan composite is developed as a non-alcoholic hand gel sanitizer formulation. Several key characterizations of the synthesized AgNPs were performed. UV–Visible spectroscopy was employed to observe the absorption peak and surface plasmon resonance of the AgNPs, as well as their interaction with oligochitosan. Fourier-transform infrared spectroscopy was used to analyze the surface characteristics and functional groups involved in the reduction of silver ions, alongside the interaction between chitosan and AgNPs. Transmission electron microscopy was utilized to examine particle size and morphology, while energy-dispersive X-ray spectroscopy was applied to determine the elemental composition. X-ray diffraction was used to identify the crystalline structure of the nanoparticles. Additionally, LC—HRMS was employed to analyze the chemical composition of the best honey used as the AgNPs bioreductor. Antibacterial activity, pH testing, syneresis testing, toxicity and primary irritation testing were conducted to assess the efficacy and safety of the hand gel sanitizer formulation. This research seeks to address the growing demand for sustainable and effective antimicrobial solutions, while contributing to the fight against antimicrobial resistance (AMR) through innovative applications of AgNPs coated with oligochitosan.

2. Material and methods

2.1. Materials and instrumentation

The chemicals used in this research were silver nitrate ($AgNO_3$, EMSURE 99 %), low-molecular-weight (LMW) chitosan (deacetylation degree 75 %–85 %; 50–190 kDa; SIGMA-ALDRICH), glacial acetic acid (CH_3COOH; 99 % EMSURE), hydrogen peroxide (H_2O_2, 30 % SMART-LAB), carbomer 940, methylparaben ($C_8H_8O_3$), infusion solution (NaCl, 0.9 %), nutrient agar (NA), barium chloride, glucose (anhydrous, Merck), fructose (powder, Merck), anthrone reagent and sulphuric acid (98 % EMSURE). The test bacteria (*Staphylococcus aureus* ATCC 25,922 and *Pseudomonas aeruginosa* ATCC 9027) were obtained from the bacterial culture, Central Laboratory of Life Sciences, Brawijaya University. Additionally, this study utilized various bioreductors, specifically cottonwood (*Ceiba pentandra*) honey, rambutan (*Nephelium lappaceum*) honey, rubber (*Hevea brasiliensis*) honey, and coffee (*Coffea* spp.) honey, all sourced from Tawon Rimba Raya Farm in Malang, East Java, Indonesia. The instruments used were UV–Vis (Shimadzu 1601 Series), FTIR (Shimadzu 8400s), EDX (Hitachi FLEXEM 1000), XRD (PANalytical X'Pert PRO), The Ultra Performance Liquid Chromatography (UPLC) LC−MS/MS system (Waters, USA) and TEM (Jeol type JEM 1400).

2.2. Synthesis of AgNPs

AgNPs were synthesized by combining 3 % honey with 0.1 M $AgNO_3$ in equal volumes, mixed thoroughly using a magnetic stirrer for 10 min at room temperature (26 °C–30 °C). Following homogenization, the solution was exposed to sunlight (88,400–137,600 lux at 26 °C–34 °C) for 10 min, resulting in the formation of AgNPs, indicated by a color change from colorless to brown. This process was repeated for each type of honey tested.

2.3. Depolymerization and deacetylation of lmw chitosan

Oligochitosan was synthesized by dissolving 0.4 g of LMW chitosan in 20 mL of 1 % acetic acid and stirring at 250 rpm for 2 h. Once fully dissolved, chitosan was depolymerized by the addition of 20 mL of 10 % H_2O_2 and stirred for an additional 2 h using a magnetic stirrer. The resulting solution was then neutralized to pH 7 using a 10 % NaOH solution (pH 13). After neutralization, the solution was filtered through filter paper, and the filtrate was collected as water-soluble chitosan (oligochitosan).

2.4. Oligochitosan coating on AgNPs

The modification of AgNPs with chitosan coating (AgNPs-Chitosan) can be achieved by mixing AgNPs with oligochitosan in a 1:1 (v/v) ratio, followed by stirring with a magnetic stirrer at 250 rpm for 2 h at room temperature. The AgNPs were added dropwise to the oligochitosan solution while stirring, until a color change was observed, from yellowish to a cloudy white appearance.

2.5. Characterization

2.5.1. UV–Vis spectroscopy

UV–Vis spectroscopy was employed to analyze the formation of AgNPs synthesized using honey as a biological reductant. The analysis was carried out using a UV–Vis spectrophotometer, with measurements taken over the range of 200 to 800 nm. The treated AgNP samples were placed in a 1 cm quartz cuvette, and absorbance was recorded at the λ_{max} corresponding to AgNPs, typically between 400 and 450 nm. Absorbance peaks within this region are indicative of surface plasmon resonance, confirming the successful formation of AgNPs.

Additionally, UV–Vis spectroscopy was applied to analyze oligochitosan and AgNPs-Chitosan composites. For the AgNPs-Chitosan complex, the introduction of oligochitosan to the AgNPs resulted in a shift and modification of the absorbance peak around 400–450 nm, reflecting the interaction between the AgNPs and oligochitosan. This shift provides evidence of the formation of a stable AgNPs-chitosan composite, suggesting successful incorporation of chitosan into the AgNP matrix.

The carbohydrate content (reducing sugars) was analyzed using the anthrone method by measuring the color change of the sample solution after reacting with anthrone reagent. A standard glucose solution with concentrations ranging from 0 to 100 ppm was prepared to generate a calibration curve through absorbance measurements using a UV–Vis spectrophotometer. The anthrone reagent was prepared by dissolving 0.1 g of anthrone in 100 mL of concentrated H_2SO_4. Honey samples were diluted, reacted with the anthrone reagent, and heated at 80 °C for 20 min until a blue-green color developed. The absorbance of the solution was measured, and the reducing sugar content was determined using the linear equation derived from the standard glucose and fructose calibration curve.

2.5.2. Fourier transform infrared (FTIR)

FTIR spectroscopy was employed to investigate the chemical composition and molecular interactions in honey, AgNPs, oligochitosan, and AgNPs-Chitosan composites. FTIR analysis of honey was performed directly without the need for freeze-drying, as honey can be analyzed in its liquid form without additional preparation. In contrast, AgNPs, oligochitosan, and AgNPs-Chitosan samples were freeze-dried prior to analysis to concentrate the materials, thereby enhancing the accuracy of the measurements and minimizing solvent effects. FTIR spectroscopy enables the detection of functional group changes and molecular interactions, such as those involved in the reduction of silver ions by honey and the formation of the AgNPs-Chitosan complex. The FTIR analysis was conducted over the wavenumber range of 400–4000 cm^{-1} at room temperature.

2.5.3. Transmission electron microscopy (TEM)

For further morphological analysis and to confirm high-resolution particle size measurements of AgNPs with distinct physical characteristics and significant differences in UV–Vis spectra, TEM was employed. The analysis was also extended to AgNPs-Chitosan samples to investigate the behavior of AgNPs within the oligochitosan matrix. AgNPs and AgNPs-Chitosan samples were prepared by dispersing them in distilled water and evenly spreading the suspension onto a carbon-coated copper grid. The grid was then dried before imaging. Observations were conducted at an accelerating voltage of 100 kV or higher to obtain high-resolution images. TEM was used to directly measure the particle size, as well as to assess the shape, distribution, and morphology of the AgNPs and AgNPs-Chitosan composites. TEM images were analyzed for particle size distribution using image analysis software, with ImageJ facilitating the measurements.

2.5.4. X-ray diffraction (XRD)

XRD was employed to confirm the crystallinity and particle size of the optimized AgNPs synthesized, based on the results of UV–Vis and FTIR analyses. XRD measurements were carried out using a CuKα X-ray source ($\lambda = 1.5418$ Å) at a scanning rate of 2°/min over a 2θ range from 10° to 90° The freeze-dried AgNPs sample were placed on a sample holder for analysis. The resulting diffraction data exhibited peaks corresponding to the standard diffraction patterns of AgNPs. These diffraction peaks were then compared with data from the JCPDS (Joint Committee on Powder Diffraction Standards) database to identify the crystalline structure of the AgNPs. The average particle size was estimated using the Scherrer equation, based on the full width at half maximum (FWHM) of the diffraction peaks.

2.5.5. Energy dispersive X-ray spectroscopy (EDX)

EDX analysis was performed on the best-performing synthetic AgNPs, selected based on prior UV–Vis and FTIR analysis. The EDX measurements were conducted using a SEM-EDX system with an accelerating voltage of 20 kV. The freeze-dried AgNPs sample was placed on a stub and analyzed with an integrated EDX detector connected to the scanning electron microscope. X-ray emissions from the sample were detected to identify the elemental composition, with characteristic X-ray peaks used to confirm the presence of silver (Ag) and other elements within the nanoparticles.

2.5.6. Liquid chromatography-high resolution mass spectrometry (LC—HRMS)

In this approach, 5 mg of the sample was dissolved in 1 mL of LC-MS grade methanol (MeOH) and then filtered through a 0.2 μm Polytetrafluoroethylene (PTFE) membrane. Separation of compounds from honey (the optimal bioreductor for AgNPs synthesis) was performed on a Vanquish Flex UHPLC-Q Exactive Plus Orbitrap High-Resolution Mass Spectrometer, coupled with an Accucore C18 column (100 × 2.1 mm, 1.5 μm, Thermo Scientific). The mobile phase consisted of 0.1 % formic acid in water (A) and 0.1 % formic acid in acetonitrile (B), with a gradient elution profile as follows: 0.0–1.0 min (15 % B), 1.0–22.0 min (15–70 % B), 22.0–24.0 min (70–95 % B), 24.0–27.0 min (95 % B), and 27.0–32.0 min (15 % B). The flow rate was set at 0.25 mL/min, with an injection volume of 2.5 μL. Ionization was performed using Electrospray Ionization (ESI) in both positive and negative modes, within the *m/z* range of 100 to 1500. Operating conditions for the ionization source were set as follows: capillary temperature at 320 °C, spray voltage at 3.8 kV, and sheath and sweep gas flow rates at 15 mL/min and 3 mL/min, respectively. The automatic gain control (AGC) was set to 3×10^6, and the injection time (IT) was fixed at 100 ms. Collision energies of 18, 35, and 53 eV were applied, and MS/MS^2 scanning was performed at a resolution of 70,000 full width at half maximum (FWHM).

2.6. Manufacturing of AgNPs-Chitosan-based hand gel sanitizer

A AgNPs-Chitosan-based hand gel sanitizer was made by mixing 0.5 g of carbomer 940 with 20 mL of distilled water in a mortar and stirring to form a gel mass. Methylparaben (0.1 g) was weighed and dissolved into 5 mL of distilled water to be added into the mortar and stirred until it reached homogeneity. A total of 5 mL of AgNPs-Chitosan as antibacterial was added to the mortar and stirred until dissolved. The gel formed was diluted by adding 20 mL of distilled water and triturated to form a gel and ensure uniformity. The resulting gel was then placed in a container for further evaluation.

2.6.1. pH test

The acidity of the hand gel sanitizer gel was measured to analyse the compatibility of the gel with human skin. The pH measurement was done by dipping the pH meter into the gel product at room temperature. A standard-compliant hand gel sanitizer has the same pH value as the skin, ranging from 4.0 to 6.5. If the pH of the hand gel sanitizer is not suitable, it can cause irritation or corrosion.

2.6.2. Syneresis test

Syneresis is the loss of water content due to evaporation from a gel material over some time. Syneresis was conducted by observing the weight of the gel before and after being placed in storage conditions at two different temperatures (5 °C and 40 °C) for 140 h

2.6.3. In vitro antibacterial activity test

The antibacterial activity was assessed using the well diffusion method on bacterial cultures in agar. Positive controls (two commercial alcohol-based hand sanitizers containing 70 % alcohol), a negative control (distilled water), 50 % v/v chitosan, and 0.1M $AgNO_3$ were tested for comparison with the various honey bioreductors of the AgNPs-Chitosan-based hand sanitizer studied in this work. Additionally, antibacterial activity tests were conducted using 70 % medical-grade alcohol, AgNPs, and AgNPs-Chitosan to provide more comprehensive results.

Sterilization of nutrient media, 0.9 % NaCl solution, and tools was done using autoclaving at 121 °C and 15 lbs for 15 min. Nutrient media (2 % NA) was prepared by boiling, cooling to 45 °C, and adding a bacterial suspension matched to McFarland 0.5 turbidity. Petri dishes were filled with 15 mL of gelatin media, and 100 μL of bacterial suspension was added. After solidification, 6 mm wells were made, and 20 μL of samples (positive and negative controls, AgNPs, AgNPs-Chitosan solutions, AgNPs-Chitosan-based hand gel sanitizers, 50 % v/v chitosan, 0.1M $AgNO_3$, and 70 % medical-grade alcohol) were added. The dishes were incubated at 37 °C for 24 h, and inhibition zones were measured using a caliper in three directions. Tests were conducted in triplicate.

2.6.4. In vivo toxicity and irritation test

The in-vivo evaluation of the AgNPs-Chitosan-based hand gel sanitizer involved a toxicity assessment using brine shrimp larvae, along with a primary irritation test conducted on the dorsal skin of rabbits. These in-vivo tests were conducted in compliance with ethical clearance No. 177-KEP-UB-2024.

The toxicity assessment using the Brine Shrimp Lethality Assay involved exposing *Artemia salina* nauplii to test solutions prepared at different concentrations. A total of 10 nauplii were introduced into each sample, and their survival was monitored after 24 h of incubation. Nauplii exhibiting no controlled forward motion during a 30-second observation period were classified as dead. The number of dead and surviving nauplii in each sample was recorded. The mortality percentage was calculated using the following Equation:

$$\% \text{ Mortality} = \frac{Number\ of\ dead\ nauplii}{Total\ nauplii\ (dead + alive)} \times\ 100$$

The mortality data obtained were used to evaluate the toxicity of the samples and to calculate the LC_{50} (the concentration required to induce 50 % nauplii mortality). The LC_{50} value serves as a key parameter for determining the relative toxicity of the tested solutions, providing a quantitative basis for toxicity comparison across samples.

The in vivo irritation test of the non-alcoholic hand gel sanitizer (AgNPs-Chitosan-based hand gel sanitizer) was conducted on adult female Australian rabbits for 72 h, with data collected every 24 h. Female rabbits had their fur removed from four distinct areas on their backs (each corresponding to a different honey bioreductor variation), with a diameter of 4 cm for each spot. To prevent potential irritation from any wounds on the shaved skin, the exposed areas were wrapped with cloth for 24 h. After this period, the skin was smeared with the reduced AgNPs-Chitosan-based hand gel sanitizer derived from each honey bioreductor. Following the application, the treated areas were again covered with cloth to prevent external contamination. The first set of data was collected 24 h after the initial application.

3. Results and discussion

3.1. Synthesis of AgNPs-Chitosan

In this study, AgNPs were synthesized via a biological method, utilizing the reduction of Ag^+ ions from $AgNO_3$ with various types of honey serving as bioreductors. Honey, primarily composed of carbohydrates such as glucose and fructose, plays a crucial role in this process. Honey can be used as a bioreductant to reduce $AgNO_3$ and form AgNPs. The sugars present in honey, particularly glucose and fructose, act as reducing agents. These sugars can be oxidized to form gluconic acid, while Ag^+ ions are reduced to form AgNPs [16,28]. These sugars, in their open-chain form, contain aldehyde and ketone groups that act as electron donors. Specifically, the carbonyl group (C=O) present in glucose or fructose (and their derivatives) can donate electrons, facilitating the reduction of Ag^+ to elemental silver (Ag^0) [36,37] (Fig. 1**a**).

During the reaction, the oxygen atom in the carbonyl group becomes negatively charged, enabling the transfer of an electron to Ag^+ ions, resulting in their reduction. This reduction process is visually confirmed by a color change in the solution—from colorless (Fig. 1**b**) to brown (Fig. 1**c**)—signifying the successful formation of AgNPs. The synthesis process involved several treatments to expedite the reaction, including stirring and exposure to direct sunlight. Stirring was employed to homogenize the solution, enhancing the likelihood of interparticle interactions and thus speeding up the reaction. Additionally, direct sunlight exposure was used to activate the aldehyde or ketone groups in the honey, facilitating the reduction of Ag^+ ions to elemental silver (Ag^0). The combined effects of stirring and sunlight accelerated the overall reduction process, improving the efficiency of AgNP formation.

Furthermore, research indicates that light intensity and exposure duration are critical factors influencing the synthesis of AgNPs, as evidenced by a correlation between the intensity of the absorbance peak and both light intensity and exposure time [36,38–40]. Specifically, blue wavelengths in sunlight provide sufficient energy to facilitate structural transformations in carbohydrates. This blue light is believed to induce tautomerization of biomolecules (from enol to keto forms), resulting in the release of reactive hydrogen

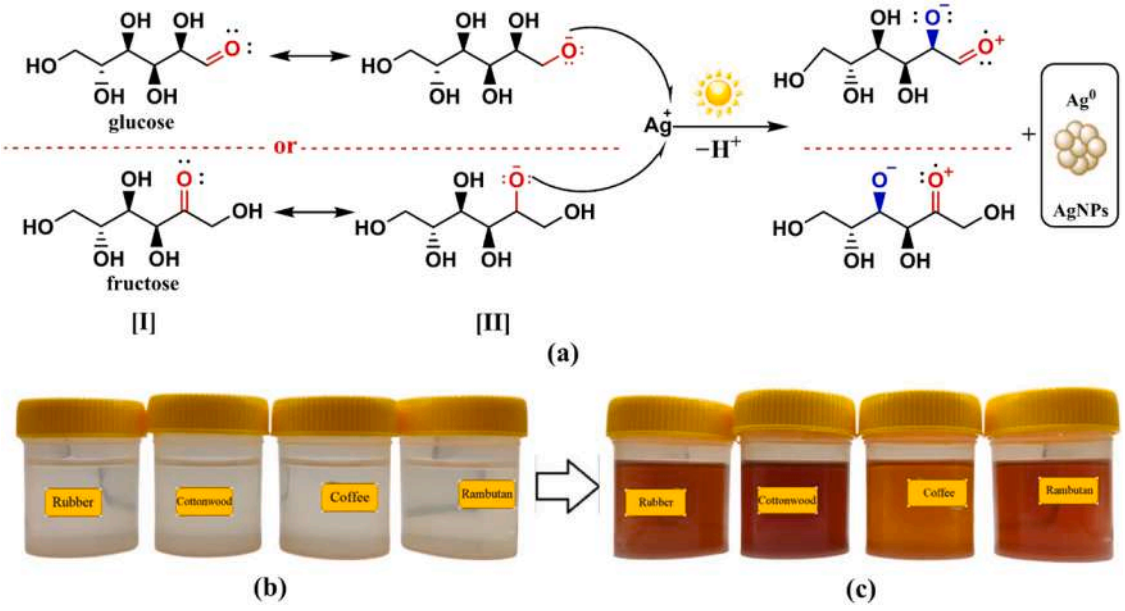

Fig. 1. Mechanism of AgNPs formulation (a); AgNPs solution before sunlight exposure (b) and after sunlight exposure (c).

atoms capable of reducing Ag ions to Ag^0 [39].

Insufficient exposure to light can lead to incomplete formation of AgNPs, often resulting in a slightly brownish product that may revert to a clear solution over time. The exact nature of the resulting product under these conditions remains unclear. However, if the sample is suspected of reverting to a reactant state, a subsequent exposure to sunlight should theoretically yield AgNPs. This was not observed, leading to the conclusion that degradation of the solution and structural damage likely occurred. Therefore, careful consideration of sunlight exposure is essential for the synthesis of more stable AgNP products.

The synthesized AgNPs exhibited distinct visual characteristics, which can be attributed to the varying reductant content present in the different types of honey used. Analysis via the anthrone method revealed reductant levels of reducing sugar in cottonwood, rambutan, rubber, and coffee honey at 79 %, 67 %, 63 %, and 48 %, respectively. These findings align with previous studies, which indicated that AgNP solutions produced with lower concentrations of bioreductors tended to display brighter colors and lower absorbance values [41–43]. This observation suggests that a reduced bioreductor concentration correlates with smaller particle sizes of the synthesized AgNPs.

The formation of AgNPs can lead to the aggregation of these particles, primarily due to their small size, which increases their reactivity and facilitates interactions with one another [44]. To mitigate the occurrence of aggregates, coating processes are employed, with chitosan polymers being a prominent choice [44,45]. Chitosan is recognized for its efficacy as a metal coating agent [46–50]. The tendency of metal nanoparticles to agglomerate is largely attributed to Van der Waals forces acting on their surfaces. By applying a chitosan coating, these attractive forces can be counteracted, enhancing the stability of AgNPs and preventing undesirable aggregation [51–53].

Chitosan is known for its solubility in acidic environments but exhibits limited solubility in water. In this research, chitosan serves a dual purpose: it acts as a coating for AgNPs in aqueous solvents and functions as a key ingredient in the formulation of water-soluble hand gel sanitizers. To enhance its solubility in water, chitosan undergoes a modification process involving depolymerization with H_2O_2. H_2O_2 is a powerful oxidizing agent that effectively degrades polysaccharides by generating hydroxyl radicals (–OH) [54]. This process results in the cleavage of glycosidic bonds within the chitosan molecule, yielding LMW chitosan, which demonstrates improved water solubility [55].

The physical transformation from long strands of LMW chitosan to oligochitosan is evident through a color change in the solution (Fig. 2). LMW chitosan typically exhibits a faint yellow hue and is only slightly soluble in water, while displaying greater solubility in acidic solvents. Upon depolymerization of LMW chitosan with H_2O_2 in acidic conditions, followed by neutralization of the pH using NaOH, chitosan oligomers (oligochitosan) are produced. This process results in a clear solution, indicating the successful conversion of LMW chitosan to oligochitosan.

During the coating reaction of AgNPs with oligochitosan, a notable color change occurs in the AgNP solution, transitioning from a brownish hue to a cloudy appearance. This color change is not merely a result of dilution; rather, it indicates the dispersion of AgNPs within the chitosan matrix, with chitosan effectively enveloping the nanoparticles surfaces [30]. The primary objective of coating AgNPs with chitosan is to enhance their stability [56,57]. Furthermore, chitosan is recognized for its excellent biocompatibility and inherent antibacterial properties, allowing it to synergize with AgNPs and significantly augment their antibacterial efficacy [58,59].

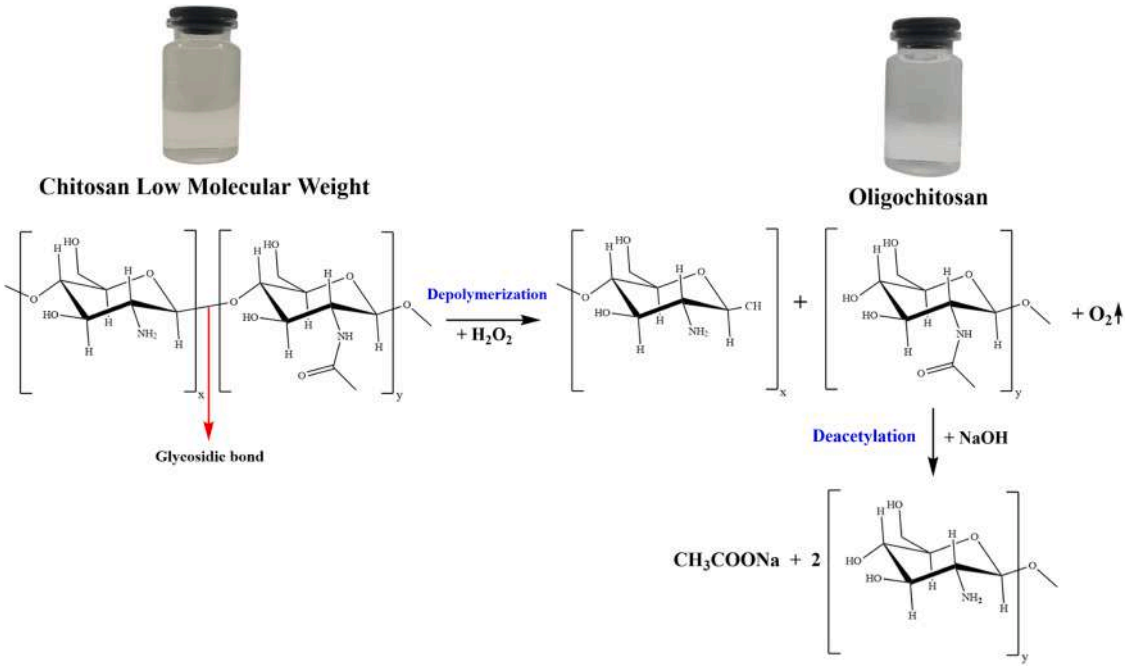

Fig. 2. Depolymerization and deacetylation of LMW chitosan (water-soluble chitosan/oligochitosan formulation).

Water-soluble chitosan, or oligochitosan, acts as a steric hindrance on the surface of AgNPs due to its positively charged amino groups (NH_2^+) [60]. This presence of chitosan enhances the stability of the nanoparticles by preventing agglomeration. The stabilization mechanism relies on the spatial separation provided by the chitosan molecules, which occupy the interstitial spaces between AgNPs. As a result, the direct contact between AgNPs is minimized, effectively inhibiting the formation of aggregates. An illustrative representation of the coating of AgNPs with chitosan is provided in Fig. 3.

3.2. Characterization of AgNPs-Chitosan

Characterization of AgNPs synthesized using various honey-based reducing agents was conducted via UV–Vis spectroscopy. The results revealed that the synthesized AgNPs exhibited a maximum absorption wavelength at 450 nm. The broad absorption peak indicated the formation of AgNPs with a range of particle size distributions [61]. Although all honey variations produced the same peak at 450 nm, there were differences in absorbance levels. Notably, darker AgNP solutions, resulting from different honey variations as reducing agents (Fig. 1**c**), showed higher absorbance values (Fig. 4). AgNPs synthesized using cottonwood honey displayed the most intense solution color and the highest absorbance at 0.94, followed by rambutan, rubber, and coffee honey with absorbances of 0.813, 0.687, and 0.653, respectively. These differences in absorbance are likely due to variations in the concentration of bioreductants present in different types of honey [42,54], as well as the pH of the reducing agents used (pH = 6.7–7.0) [62].

The optical properties of AgNPs, such as their maximum absorption wavelength, directly influence the particle size produced [63]. Larger particles, often resulting from aggregation, exhibit higher absorbance wavelengths [56]. Beyond optical characteristics, particle size also significantly impacts the biological activity of AgNPs, particularly their antibacterial efficacy. This relationship is attributed to the specific surface area of AgNPs—smaller particles have a larger surface area, which enhances their antibacterial performance by increasing the likelihood of interaction with bacterial cells [57].

Upon coating the AgNPs with oligochitosan, a significant shift in the UV–Vis spectrum was observed, marked by the disappearance of the characteristic surface plasmon resonance (SPR) peak of AgNPs at 450 nm, which was replaced by a spectrum resembling that of oligochitosan. This spectral change indicates successful encapsulation of the AgNPs within the oligochitosan matrix, leading to a modification of the nanoparticles' optical properties. The disappearance of the SPR peak can be attributed to the formation of a stable chitosan layer that prevents direct interaction between the AgNPs and light. Typically, the SPR peak arises from the collective oscillation of conduction electrons on the nanoparticle surface, but the chitosan coating obstructs this interaction, resulting in quenching of the SPR signal.

Furthermore, the chitosan matrix effectively isolates the AgNPs, minimizing interparticle interactions and preventing aggregation, which typically enhances the SPR signal due to nanoparticle coupling. The lack of this effect in the coated AgNPs suggests that oligochitosan not only encapsulates but also stabilizes the nanoparticles, producing a spectrum more representative of oligochitosan than the AgNPs themselves.

Among the four types of honey used as bioreductors—cottonwood, rambutan, rubber, and coffee—AgNPs synthesized with cottonwood honey exhibited the most prominent results. The UV–Vis spectra of AgNPs reduced with cottonwood honey displayed significantly higher absorbance, indicating a higher concentration of nanoparticles. After capping with oligochitosan, the absorbance of the AgNP-oligochitosan composite showed a marked decrease, resulting in a flatter spectrum closely resembling that of pure oligochitosan. This decrease in peak absorbance confirms the successful capping process, where oligochitosan effectively encapsulates the AgNPs.

In contrast, AgNPs reduced with rambutan honey exhibited lower absorbance compared to cottonwood honey. However, after capping with oligochitosan, the AgNP-oligochitosan spectrum still showed relatively high absorbance, but it did not resemble the oligochitosan spectrum, indicating suboptimal interaction between AgNPs and oligochitosan. Similarly, AgNPs reduced with rubber and coffee honeys displayed lower absorbance peaks, but after capping with oligochitosan, their spectra became more similar to that of oligochitosan, suggesting better interaction between AgNPs and oligochitosan. However, the lower absorbance of these AgNPs suggests fewer nanoparticles were synthesized.

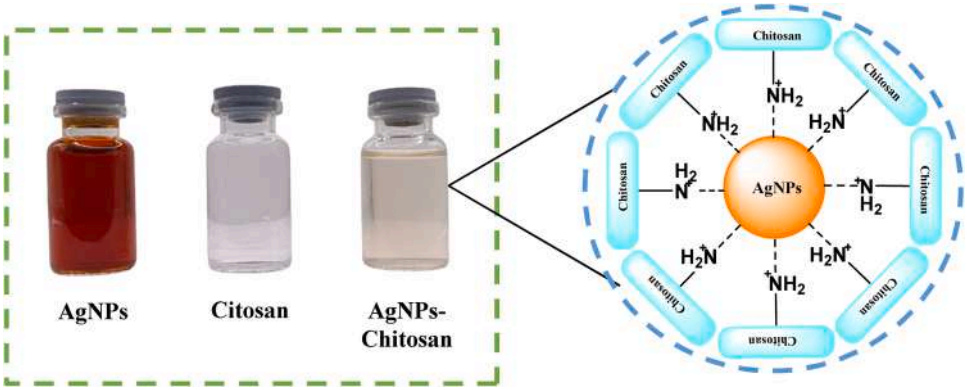

Fig. 3. Solutions of AgNPs, Chitosan, and AgNPs-Chitosan, along with an Illustration of Chitosan Coating on the Surface of AgNPs.

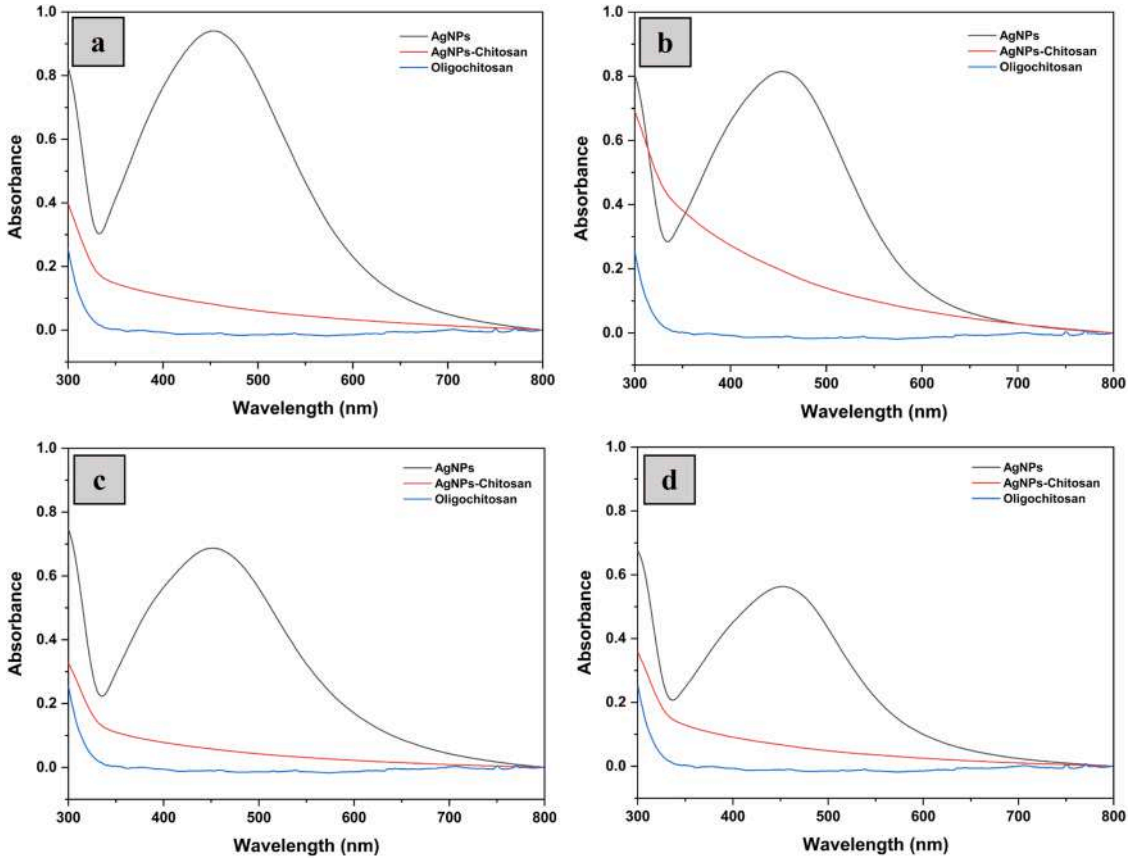

Fig. 4. Characterization of AgNPs with bioreductors of cottonwood honey (a), rambutan honey (b), rubber honey (c) and coffee honey (d) using a UV–Vis instrument.

Overall, cottonwood honey demonstrated superior performance in the synthesis of AgNPs and AgNP-oligochitosan composites. The higher absorbance observed in AgNPs synthesized with cottonwood honey indicates a larger number of AgNPs formed, likely due to more efficient reduction of Ag^{+} to Ag^{0}, possibly attributed to a higher concentration of reducing compounds in the honey. Additionally, the similarity in surface plasmon resonance (SPR) patterns to oligochitosan suggests that cottonwood honey facilitates optimal interaction between AgNPs and oligochitosan. The stronger absorbance further implies that the combination of cottonwood honey and oligochitosan yields more effective AgNP-oligochitosan composites.

FTIR analysis was conducted to investigate the interaction between the formation of AgNPs and the honey bioreductors, as well as the capping process of oligochitosan on AgNPs (Fig. 5). Several absorption peaks appeared within the broad region of 3000–3500 cm^{-1}, with high intensity, indicating the presence of O—H groups in the honey, AgNPs, and AgNPs-Chitosan samples, as well as NH groups in the oligochitosan sample. These functional groups likely originate from phenolic compounds, flavonoids, or proteins in the honey, including glucose and fructose, which serve as the primary bioreductants during AgNP synthesis. Additionally, low-intensity absorption bands around 2930 cm^{-1} in the honey, AgNPs, and AgNPs-Chitosan samples correspond to C—H bonds from the organic compounds present in the honey.

Shifts, peak splitting, and intensity reductions were observed in the AgNPs sample compared to the honey samples in the 1640–1730 cm^{-1} range, indicating modifications in the carbonyl (C=O) groups of aldehydes (glucose) and ketones (fructose). This suggests that the formation of AgNPs involves electron donation from these carbonyl groups. Furthermore, the change in intensity from 1560 to 1570 cm^{-1} (oligochitosan) to a lower intensity in the AgNPs-Chitosan sample reflects interactions between the amino (NH_2^{+}) groups of oligochitosan and the surface of the AgNPs. This result demonstrates that the capping interaction of AgNPs with oligochitosan occurs through the amino groups of oligochitosan, as illustrated in Fig. 3.

Additionally, peaks in the 1390–1405 cm^{-1} range in both oligochitosan and AgNPs-Chitosan samples correspond to C—O-C bonds in cyclic structures. Moreover, the peak observed at 1300–1310 cm^{-1} in the AgNPs spectrum, which is absent in the honey samples (cottonwood, rambutan, rubber, and coffee), can be interpreted as C—O or C—H vibrations, indicating the presence of organic components from honey that act as stabilizers on the AgNPs surface, preventing aggregation and contributing to nanoparticle stability.

Finally, the peaks in the 1000–1050 cm^{-1} region for honey, AgNPs, and AgNPs-Chitosan are associated with functional groups linked to hydroxyl (-OH) or C—O vibrations, likely originating from sugars or other organic compounds, such as polysaccharides or phenolic compounds found in honey. These compounds play a role in AgNP formation. Overall, the FTIR spectra highlight the presence

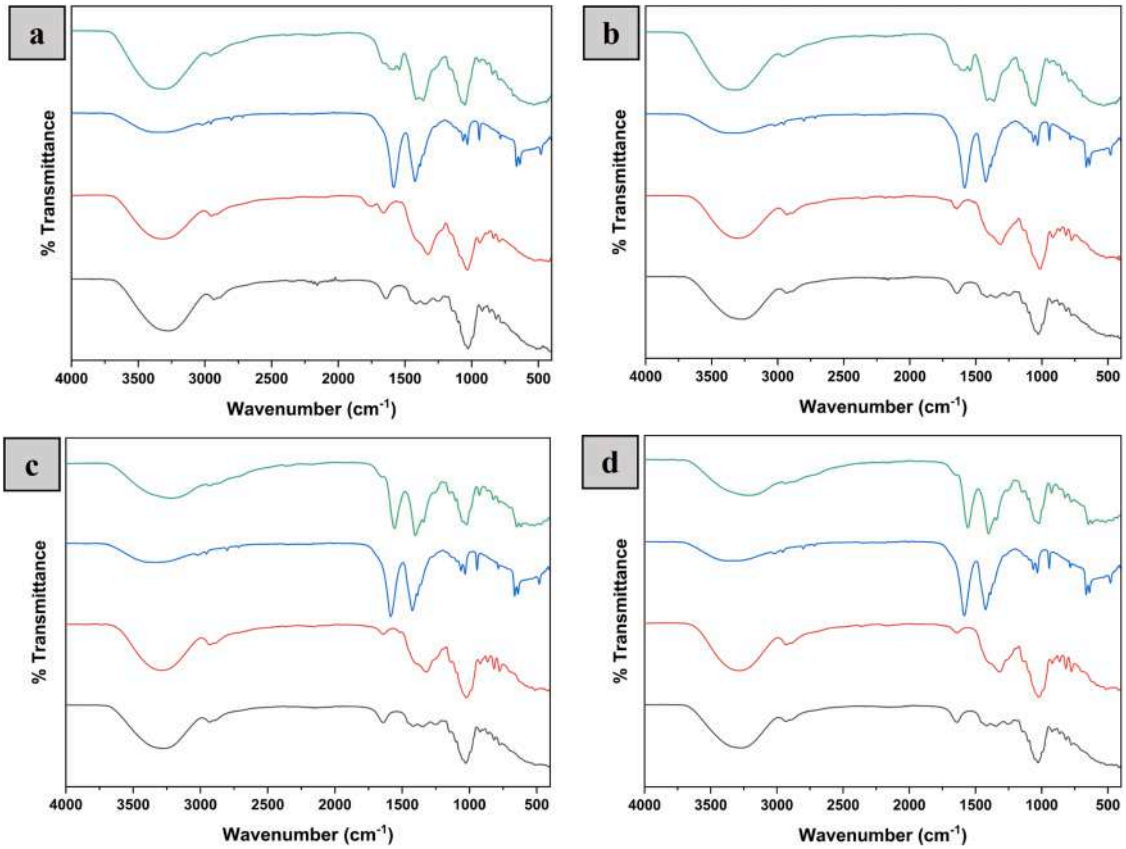

Fig. 5. The FTIR Spectra of Honey (black); AgNPs (red); Oligochitosan (blue); AgNPs-Chitosan (green) with Different Bioreductor of Cottonwood Honey (a); Rambutan Honey (b); Rubber Honey (c); and Coffee Honey (d).

of various organic functional groups from honey, which interact with the AgNPs surface, playing a crucial role in nanoparticle stabilization and influencing the physicochemical properties and biological activity of the synthesized AgNPs.

Among the four types of honey used as bioreductors, AgNPs synthesized with cottonwood honey exhibited the strongest interactions, both in terms of AgNP formation and subsequent interaction with oligochitosan to form AgNPs-Chitosan composites. This interaction is clearly evidenced by the emergence of new or overlapping bands at 1639 cm^{-1} and 1730 cm^{-1} in the AgNP spectrum,

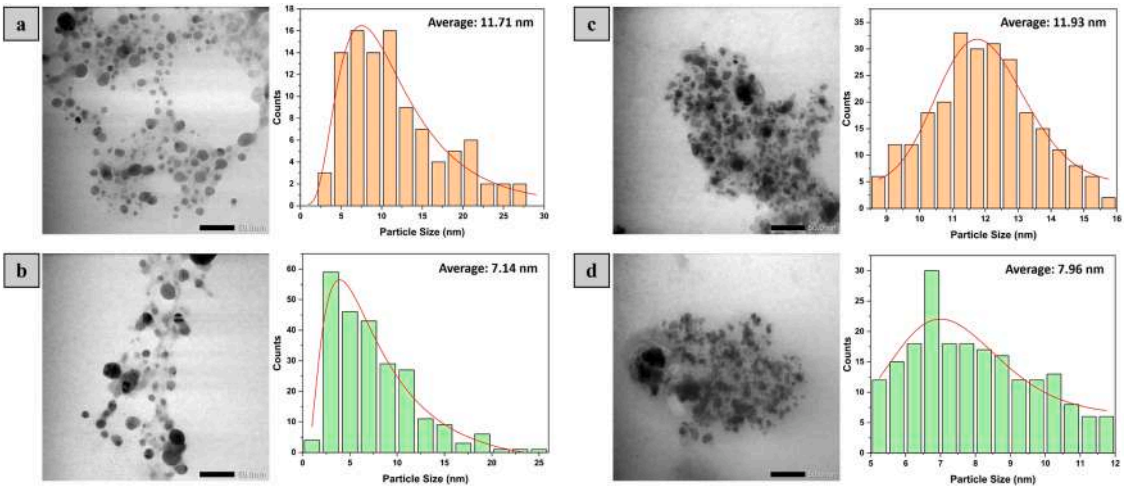

Fig. 6. Measurement of AgNPs with bioreductor of cottonwood honey (a) and coffee honey (b); AgNPs-Chitosan with bioreductor of cottonwood honey (c) and coffee honey (d) using TEM analysis.

whereas the cottonwood honey sample itself displayed only a peak at 1643 cm^{-1}, indicating that AgNPs were reduced via carbonyl (C=O) groups. Additionally, a significant decrease in intensity was observed in the 1560–1570 cm^{-1} range in the AgNPs-Chitosan sample, where high intensity was previously observed in the oligochitosan spectrum. This decrease in intensity suggests a strong interaction between cottonwood-reduced AgNPs and oligochitosan through amino (NH_2^+) groups. In contrast, the other honey samples (rambutan, rubber, and coffee) exhibited weaker interactions, with only minor changes in peak intensities, indicating less significant interactions between the bioreductors and AgNPs, as well as between AgNPs and oligochitosan.

TEM was performed specifically on AgNPs synthesized using cottonwood and coffee honey (Fig. 6) because these samples exhibited the most distinct optical characteristics—cottonwood honey produced the most concentrated solution, while coffee honey resulted in the brightest. This choice was made to maximize the contrast in optical properties, as significant differences in color can indicate variations in particle size, shape, and distribution. Analyzing samples with the most pronounced optical differences helps in understanding how these parameters are influenced by the synthesis conditions and bioreductor source. TEM provides detailed insights into the morphology and size of the particles, which is crucial for linking optical behavior (like color intensity and hue) to specific physical characteristics. Focusing on the samples with the most distinct optical variations ensures that the relationship between visual cues and nanoscale structure is clearly established, enhancing the validity of correlations drawn between the optical properties and the physical characteristics of the AgNPs.

For the AgNPs synthesized with cottonwood honey, the average particle diameter was found to be 11.71 nm, with a broad size distribution ranging from 3 to 27 nm. This indicates that cottonwood honey as a bioreductant produced AgNPs with a relatively larger size and a broader size distribution. In contrast, AgNPs synthesized with coffee honey exhibited a smaller average particle size of 7.14 nm, with a narrower distribution between 3 and 23 nm. These findings suggest that the color of the AgNPs colloidal solutions, which are influenced by the bioreduction process, can provide valuable estimates regarding particle size. Additionally, the uniformity of the particles was higher in the coffee honey-reduced AgNPs, as reflected by the R^2 value of 0.95827, compared to the cottonwood honey-reduced AgNPs, which had a lower R^2 value of 0.9344. The R^2 values represent the degree of uniformity in the particle size distribution, where values closer to 1 indicate greater uniformity, as evidenced by the narrower peaks in the distribution data.

When the AgNPs were further coated with chitosan to improve their stability and functionality, a new comparison was made. The AgNPs synthesized using cottonwood honey and coated with chitosan had an average particle size of 11.93 nm, slightly larger than the AgNPs synthesized with coffee honey (7.96 nm). Despite this, the particle size distribution of AgNPs reduced with cottonwood honey became more uniform when incorporated into the chitosan matrix, with an R^2 value of 0.9487, compared to the coffee honey-reduced AgNPs, which had a much lower R^2 value of 0.7745. This suggests that the chitosan coating may have a stabilizing effect on the AgNPs, particularly those synthesized with cottonwood honey, enhancing their uniformity. The greater size uniformity of the cottonwood honey-reduced AgNPs in the chitosan matrix may be attributed to specific interactions between the honey components and chitosan, potentially leading to more efficient particle stabilization. In contrast, the less uniform particles observed in the coffee honey-reduced AgNPs suggest that chitosan may not interact as effectively with these smaller particles or with the components of coffee honey.

The TEM image reveals the presence of two distinct layers in the AgNPs-chitosan sample: an inner core of silver nanoparticles (AgNPs) and an outer layer of chitosan encasing the core. The chitosan coating, with a thickness ranging from 6 to 8 nm, indicates the successful formation of protective layer. This layer results from interactions between the functional groups of chitosan, such as amino groups, and the surface of AgNPs, creating a stable shell around the nanoparticles. The chitosan layer plays a crucial role in stabilizing AgNPs, preventing aggregation through electrostatic and steric interactions. Moreover, the chitosan enhances the biocompatibility of AgNPs due to its inherent biocompatible and antibacterial properties, making the composite more suitable for medical and pharmaceutical applications. The distinct two-layer structure demonstrates chitosan's effectiveness as a coating agent, providing both

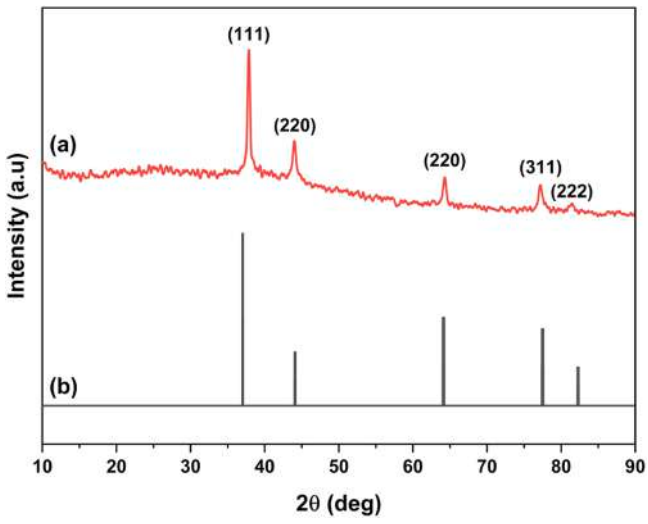

Fig. 7. XRD pattern of AgNPs with cottonwood honey bioreductor (a); and AgNPs Standard (JCPDS: 04–0783) (b).

stability and functional versatility to the AgNPs for a range of potential applications.

These findings highlight the crucial roles of both the reducing agent (type of honey) and the stabilizing agent (oligochitosan) in regulating the size, distribution, and uniformity of AgNPs. Chitosan coating appears to enhance the uniformity of AgNPs, particularly those reduced with cottonwood honey, likely due to better particle interactions and stabilization, leading to a more homogeneous distribution compared to AgNPs reduced with coffee honey. This observation aligns with UV–Vis and FTIR spectra, which indicate that AgNPs synthesized using cottonwood honey exhibit stronger interactions with the oligochitosan coating than those reduced with other types of honey, such as rambutan, rubber, or coffee honey. Consequently, further characterization of the crystal structure was performed using XRD, and sample purity was assessed with EDX specifically for AgNPs synthesized with cottonwood honey. Additional analyses using LC—HRMS were also conducted to identify the specific components present in cottonwood honey.

The crystal structure of AgNPs was characterized using XRD, as presented in Fig. 7. The XRD pattern of the AgNPs synthesized with cottonwood honey aligns with the standard reference for AgNPs (JCPDS code No. 04–0783). The diffractogram shows prominent peaks at 2θ angles of 37.84°, 44.05°, 64.31°, 77.14°, and 81.40°, which correspond to the Bragg reflections from the (111), (200), (220), (311), and (222) planes of the face-centered cubic (FCC) lattice of silver.

The Debye-Scherrer equation was employed to estimate the size of the AgNP crystals, focusing on the peak with the highest intensity observed at $2\theta = 37.84°$ This particular peak was chosen as it represents the most prominent and sharp feature in the XRD pattern, making it the most reliable for size estimation. Peaks with the highest intensity generally provide the most definitive information regarding the crystal structure, as they are less likely to be influenced by impurities or secondary phases. Using this peak and an FWHM of 0.1673°, the estimated crystallite size for AgNPs synthesized from cottonwood honey is approximately 50.22 nm.

Fig. 8 presents the EDX spectrum of the AgNPs. The characteristic peak for AgNPs was observed at approximately 3 keV, consistent with earlier studies [64]. The analysis revealed a high purity of AgNPs, with silver atoms comprising about 84 % of the sample. The remaining 16 % was attributed to oxygen, likely originating from the air, residual bioreductants, or the $AgNO_3$ used in the synthesis.

Notably, no carbon was detected in the sample, which can be attributed to several factors. First, the AgNPs underwent a freeze-

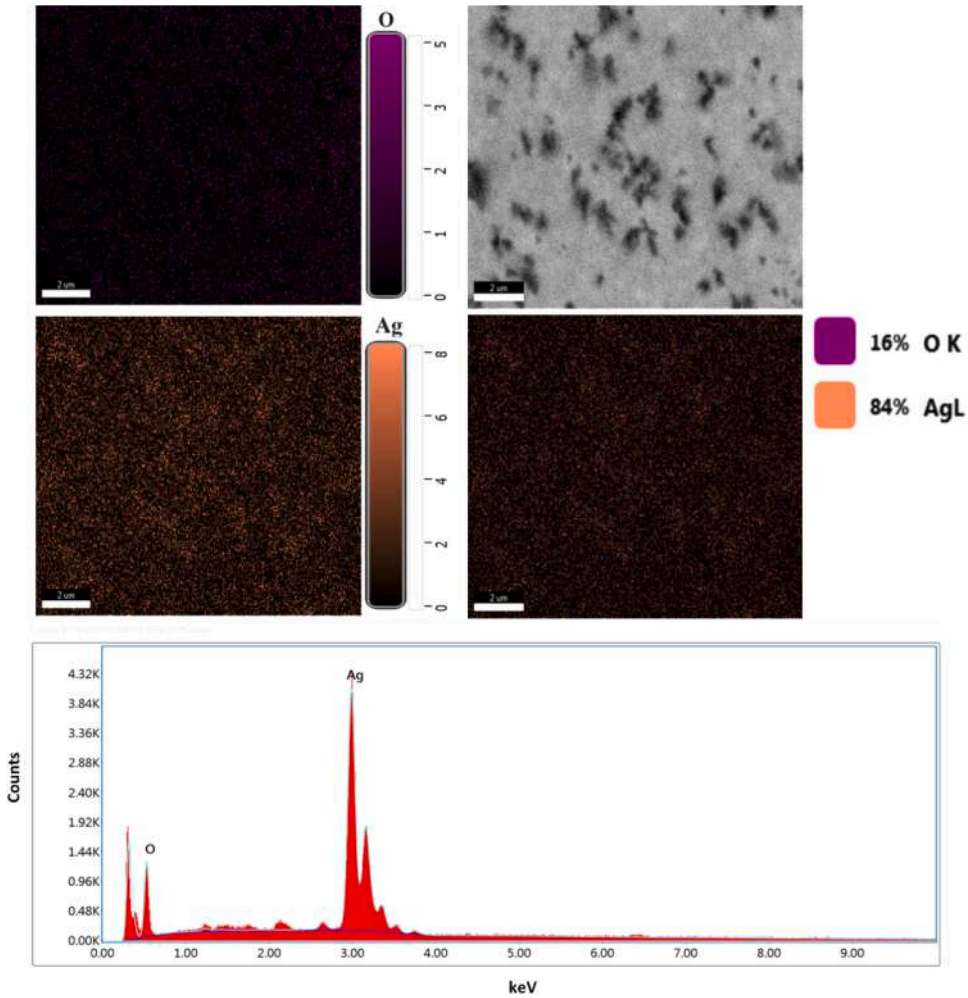

Fig. 8. EDX pattern of AgNPs with cottonwood honey bioreductor.

drying process, which effectively removed any organic solvents and minimized the presence of carbon-based residues. Additionally, a relatively low concentration of the bioreductant was used in the synthesis, reducing the likelihood of carbon contamination from organic compounds. The weak bioreductant concentration means that only minimal organic material remained on the AgNPs' surface, contributing to the absence of a detectable carbon signal in the EDX analysis. This supports the conclusion that the synthesized AgNPs are of high purity, with minimal organic interference.

The honey derived from *C. pentandra* was analyzed using LC—HRMS to identify its constituent compounds, particularly the carbohydrate fractions commonly present in honey, which may serve as bioreductants in the synthesis of AgNPs. The carbohydrate profile of the honey predominantly consists of glucose and fructose, with glucose concentrations ranging from 35.99 % to 42.57 % and fructose concentrations ranging from 24.63 % to 35.06 % [65]. Based on the LC—HRMS spectrum (Fig. 9), we focused on the retention time range of 0–2 min, considering that the peak in this region exhibits a relative abundance approaching 99.99 %, indicating that the substances or compounds detected within this timeframe are the primary components of the sample. Consequently, this peak is more relevant for analysis and provides more significant information. In contrast, peaks at longer retention times (2–33 min) tend to exhibit lower intensities and can be regarded as noise, potentially resulting from contamination, instrument interference, or other disturbances unrelated to the analytical objective.

The LC—HRMS analysis identified several carbohydrate (Table 1) derivatives of glucose and fructose, each originating from specific modifications of these sugars. Glucoheptonic acid results from the oxidation of glucose at the terminal CH_2OH group, converting it into a carboxyl group. Similarly, d-gluconic acid is formed by the oxidation of the aldehyde group at C1 of glucose, resulting in a carboxyl group. The lactone form of d-gluconic acid, known as d-glucono-delta-lactone, forms when the carboxyl group reacts with the hydroxyl group at C5, creating a cyclic ester. Lactobionic acid is derived from d-gluconic acid by the addition of a galactose molecule, forming a disaccharide. d-glucopyranuronic acid is another glucose derivative resulting from oxidation at the C6 position, converting the CH_2OH group into a carboxyl group, forming a uronic acid. 4-O-methyl-alpha-d-glucuronic acid is a methylated version of glucuronic acid, where the hydroxyl group at C4 is replaced with a methoxy group, a modification commonly found in glycosaminoglycans. Methyl-N-(beta-d-glucopyranosyl)oxamate is a glucose derivative where a glucopyranosyl group is attached to an oxamate moiety through methylation, likely occurring through glucose conjugation in various metabolic processes.

On the fructose side, Hex-2-ulose is a ketohexose derivative of fructose, formed by the isomerization of fructose, where the aldehyde group is converted into a ketone at the C2 position, giving it a ketose structure. Finally, d-sucrose, a disaccharide composed of one glucose molecule and one fructose molecule, forms through a condensation reaction where the glucose and fructose units are joined by a glycosidic bond between the C1 of glucose and the C2 of fructose. Each of these derivatives highlights how glucose and fructose undergo various biochemical modifications, resulting in bioactive compounds with diverse chemical structures and functional properties.

Although these compounds are detected in their derivative forms, this does not impact the outcomes of our study, as the derivatization of glucose and fructose in honey continues to reflect their essential role in the bioreduction process. These modified forms do not alter the overall functionality of honey as a reducing agent for AgNPs. Given their chemical properties, these carbohydrate derivatives retain the potential to reduce silver ions (Ag^+) and facilitate the formation of AgNPs in honey-based synthesis processes.

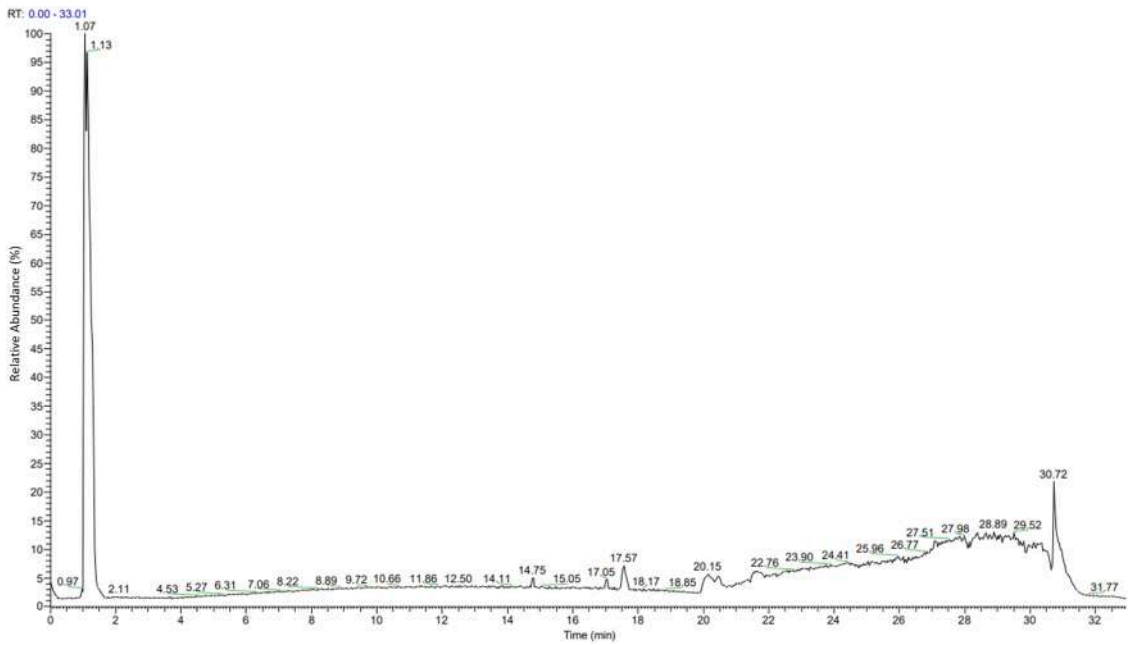

Fig. 9. The LC—HRMS chromatogram of Cottonwood (*C. Pentrandra)* Honey.

Table 1
LC-MS of Cottonwood (*C. Pentrandra)* Honey.

No	RT	Name	DB Formula	Area
Primary Metabolite				
Alkaloid				
1	1.091	5,9-Dihydroxy-2-(2-hydroxy-2-propanyl)−1-(1-hydroxy-3,5,6-trimethoxy-10-methyl-9-oxo-9,10-dihydro-2-acridinyl)−10-methoxy-11-methyl-1,11-dihydrofuro[2,3-c]acridin-6(2H)-one	$C_{37}H_{36}N_2O_{11}$	598,821,449.3
Terpenoid				
2	1.095	2-C-methylerythritol 4-phosphate	$C_5H_{13}O_7P$	467,265,531.6
3	10.669	(±)-Camphoric acid	$C_{10}H_{16}O_4$	21,880,518.74
Alcohol				
4	1.09	Hexitol	$C_6H_{14}O_6$	38,902,679.27
Secondary Metabolite				
Carbohydrate				
5	1.116	Hex-2-ulose	$C_6H_{12}O_6$	3,664,130,206
6	1.118	Glucoheptonic Acid	$C_7H_{14}O_8$	2,869,537,559
7	1.111	D-Sucrose	$C_{12}H_{22}O_{11}$	1,457,225,161
8	1.079	D-Gluconic acid	$C_6H_{12}O_7$	441,880,060.9
9	1.144	D-Glucono-delta-lactone	$C_6H_{10}O_6$	194,340,823.9
10	1.21	d-Erythro-l-gluconolactone	$C_9H_{18}O_9$	161,160,637
11	1.12	Maltotriose	$C_{18}H_{32}O_{16}$	96,493,638.52
12	1.087	Lactobionic acid	$C_{12}H_{22}O_{12}$	79,407,916.57
13	1.113	D-Arabinose	$C_5H_{10}O_5$	71,261,708.26
14	1.068	D-Glucopyranuronic acid	$C_6H_{10}O_7$	68,864,934.59
15	1.18	2-(alpha-d-mannosyl)-d-glyceric acid	$C_9H_{16}O_9$	66,892,836.43
16	1.188	4-O-Methyl-alpha-d-glucuronic acid	$C_7H_{12}O_7$	62,153,108.37
17	1.071	Methyl-N-(beta-d-glucopyranosyl)oxamate	$C_9H_{15}NO_8$	49,145,625.75
18	1.057	(2R,3S,4S,5S,6R)−6-[(2R,3S,4R,5S,6R)−6-(3-aminopropoxy)−2-carboxy-4,5-dihydroxyoxan-3-yl]oxy-3,4,5-trihydroxyoxane-2-carboxylic acid	$C_{15}H_{25}NO_{13}$	24,450,227.32
19	1.144	deoxyxylulose monophosphate	$C_5H_{11}O_7P$	21,165,036.48
20	1.122	Hexopyranosyl-(1->4)hexopyranosyl-(1->4)hexopyranosyl-(1->4)hexopyranose	$C_{24}H_{42}O_{21}$	20,930,236.57
21	1.108	1,4-d-xylobiose	$C_{10}H_{18}O_9$	18,904,532.8
22	1.463	3-O-beta-d-galactosyl-sn-glycerol	$C_9H_{18}O_8$	16,650,217.09
23	1.173	3-O-(N-Acetylneuraminyl)galactose	$C_{17}H_{29}NO_{14}$	8,312,687.622
Fenolat				
24	1.131	ethyl (2S)−2-[[[(E)−2-[2-[(2-amino-6-oxo-1H-purin-9-yl)methyl]phenyl]ethenyl]-phenoxyphosphoryl]amino]propanoate	$C_{25}H_{27}N_6O_5P$	57,412,679.34
Other Compound				
25	1.102	[(2R,3S,4R,5R)−5-[5-amino-4-(prop-2-enylcarbamoyl)imidazol-1-yl]−3,4-dihydroxyoxolan-2-yl]methyl dihydrogen phosphate	$C_{12}H_{19}N_4O_8P$	272,561,078
26	1.1	[(3S,4R)−5-(3-carbamoyl-1,2,4-triazol-1-yl)−3,4-dihydroxyoxolan-2-yl]methyl 2-(2-methoxyethoxy) acetate	$C_{13}H_{20}N_4O_8$	122,298,565
27	1.153	2′,3′,5′-triacetyl-5-Azacytidine	$C_{14}H_{18}N_4O_8$	60,457,664.04

3.3. Hand gel sanitizer product testing

3.3.1. pH test

The pH of the hand gel sanitizer gel formulations was assessed using a pH meter, with measurements taken for each variation of the AgNP bioreductors. The pH values across all formulations ranged from 4.0 to 4.3. This acidity level reflects the concentration of H^+ ions in the solution, which is influenced by the protonation of hydroxyl groups from AgNPs-Chitosan and one hydroxyl group from $C_8H_8O_3$.

Table 2
Syneresis test results of AgNPs-Chitosan-based hand gel sanitizer on brine shrimp larvae with different AgNPs reducing agents.

Bioreductor of AgNPs	0 h	72 h		144 h		216 h	
	GM (gr)	GML (gr)	GML (%)	GML (gr)	GML (%)	GML (gr)	GML (%)
Storage temperature: 5 °C							
Cottonwood honey	19.65	0.02	0.10	0.04	0.20	0.05	0.25
Rambutan honey	19.66	0.03	0.15	0.05	0.25	0.08	0.41
Rubber honey	19.71	0.01	0.05	0.03	0.15	0.05	0.25
Coffee honey	19.75	0.02	0.10	0.03	0.15	0.06	0.30
Storage temperature: 40 °C							
Cottonwood honey	19.62	0.12	0.61	0.22	1.12	0.33	1.68
Rambutan honey	19.66	0.14	0.71	0.31	1.58	0.48	2.44
Rubber honey	19.69	0.11	0.56	0.28	1.42	0.41	2.08
Coffee honey	19.72	0.12	0.61	0.32	1.62	0.45	2.28

Note: GM, gell mass; GML, gell mass loss.

A pH range of 4.0 to 7.0 is considered safe for the skin, aligning with ideal standards to mitigate inflammation and irritation, with optimal conditions observed at a pH below 5.0 [66]. Research indicates that the growth of certain pathogenic bacteria associated with skin infections occurs most readily in neutral to alkaline pH environments, whereas a more acidic pH poses greater challenges for bacterial survival.

3.3.2. Syneresis test

Syneresis testing of the hand gel sanitizer products (Table 2) was conducted at both cold (5 °C) and elevated (40 °C) storage temperatures to evaluate the gel's stability under these conditions. The syneresis test assesses the gel's ability to retain its structure when subjected to temperature-induced changes, which can result in liquid exudation and gel contraction or degradation [67,68]. In general, a very low gel mass loss (<5 %) over an extended testing period of more than 7 days (168 h) is indicative of good gel stability [69]. The findings indicate that hand gel sanitizer gels stored at lower temperatures exhibited superior resistance compared to those stored at higher temperatures. The gel mass loss for products kept at cold temperatures ranged from 0.25 % to 0.41 %, whereas the loss for those at warmer temperatures was notably higher, ranging from 1.68 % to 2.28 % over a 216-hour period. This difference can be attributed to the effects of temperature, with higher storage temperatures facilitating the escape of water from the gel matrix. Elevated temperatures can accelerate the disruption of hydrogen bonds within the gel, leading to the formation of smaller, lighter compounds that are more prone to evaporation [68].

3.3.3. In vitro antibacterial activity test

Antibacterial assays (Tables 3 and Fig. 10) were performed using distilled water as a negative control, which exhibited no antibacterial activity. Interestingly, the positive control, a commercial hand gel sanitizer containing 70 % alcohol, also showed no antibacterial efficacy against the two bacterial strains tested. In contrast, $AgNO_3$ (0.1 M) and chitosan (2 %) demonstrated significant antibacterial activities, with inhibition zones measuring 10.13 ± 0.87 mm and 21.15 ± 2.01 mm against *S. aureus*, and 13.84 ± 0.71 mm and 23.94 ± 1.74 mm against *P. aeruginosa*, respectively. Various types of honey were assessed for their antibacterial properties; however, none of the four honey types exhibited any measurable antibacterial activity against the tested bacteria. Notably, honey displayed minimal antibacterial effects against *S. aureus*, but the observed activity was insufficient to produce a discernible inhibition zone.

Testing the antibacterial activity of AgNPs synthesized with various honey bioreductors yielded promising results, although the differences were not statistically significant. The inhibition zones observed against *S. aureus* for the AgNPs produced with cottonwood, rambutan, rubber, and coffee honey were 15.47 ± 0.18 mm, 15.60 ± 0.28 mm, 15.76 ± 0.24 mm, and 15.92 ± 0.23 mm, respectively. For *P. aeruginosa*, the inhibition zones measured 13.94 ± 0.72 mm, 14.47 ± 0.82 mm, 14.61 ± 0.76 mm, and 15.45 ± 0.88 mm, respectively. TEM analysis revealed that AgNPs synthesized with coffee honey exhibited a smaller average particle size of 7.14 nm compared to 11.71 nm for those produced with cottonwood honey. While the smaller particle size correlated with slightly enhanced antibacterial activity, the differences were not substantial. This increased activity is due to the larger surface area of smaller AgNPs, enhancing their interaction with bacterial cell components [70].

AgNPs synthesized using honey as a bioreductant exhibit superior antibacterial activity compared to those produced with other bioreductants reported in previous studies (Table 4**)**. Against *S. aureus*, AgNPs derived from honey achieved an inhibition zone of 15.92 ± 0.23 mm, outperforming *S. polyanthum* (13.00 ± 1.32 mm), *A. vera* (14.3 ± 0.6 mm), and *A. platensis* (14 ± 0.4 mm). The honey-based AgNPs also demonstrated significantly higher efficacy than *H. ulmarius* (4.1 ± 0.2 mm) and *P. americana* (5.25 ± 0.35 mm). Only

Table 3
The inhibition zone data of antibacterial activity test.

Code	Sample Type		Inhibition Zones (mm)	
			S. aureus	*P. aeruginosa*
1	Control	$AgNO_3$ 0.1M	10.13 ± 0.87	13.84 ± 0.71
2		Control (+)	6 ± 0	6 ± 0
3		Control (-)	6 ± 0	6 ± 0
4		Chitosan 2 %	21.15 ± 2.01	23.94 ± 1.74
1	Honey	Cottonwood	6 ± 0	6 ± 0
2		Rambutan	6 ± 0	6 ± 0
3		Rubber	6 ± 0	6 ± 0
4		Coffee	6 ± 0	6 ± 0
1	AgNPs	Cottonwood	15.47 ± 0.18	13.94 ± 0.72
2		Rambutan	15.60 ± 0.28	14.47 ± 0.82
3		Rubber	15.76 ± 0.24	14.61 ± 0.76
4		Coffee	15.92 ± 0.23	15.45 ± 0.88
1	AgNPs-Chitosan	Cottonwood	30.14 ± 0.85	21.11 ± 0.36
2		Rambutan	27.22 ± 1.60	20.77 ± 1.40
3		Rubber	26.61 ± 1.21	20.67 ± 0.58
4		Coffee	26.30 ± 1.56	19.85 ± 0.83
1	Hand gel sanitizer based AgNPs-Chitosan	Cottonwood	13.81 ± 0.54	9.89 ± 0.06
2		Rambutan	12.24 ± 1.13	11.16 ± 0.73
3		Rubber	14.84 ± 0.34	10.91 ± 0.67
4		Coffee	13.14 ± 1.49	10.92 ± 1.58

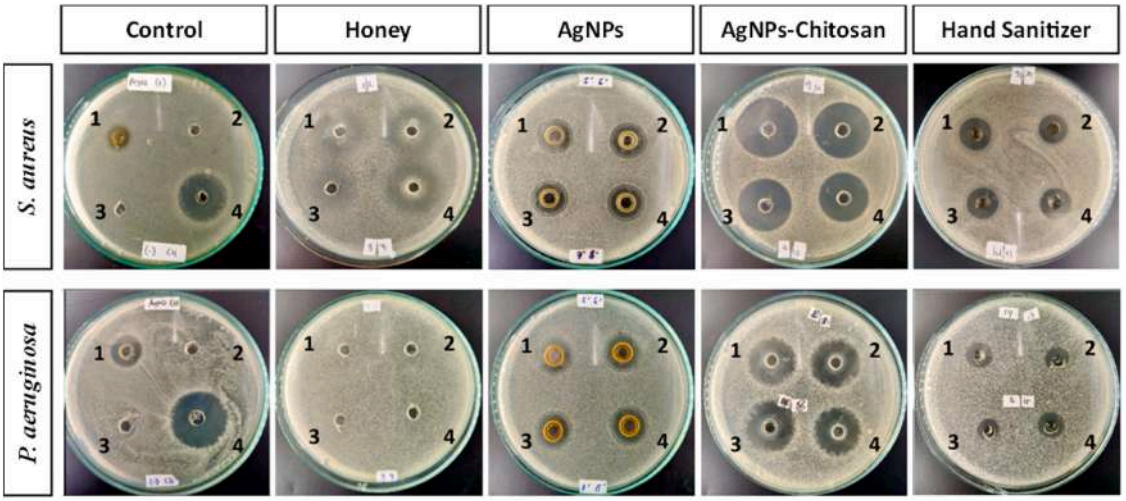

Fig. 10. The antibacterial activity test was conducted, and the results are presented in Table 3.

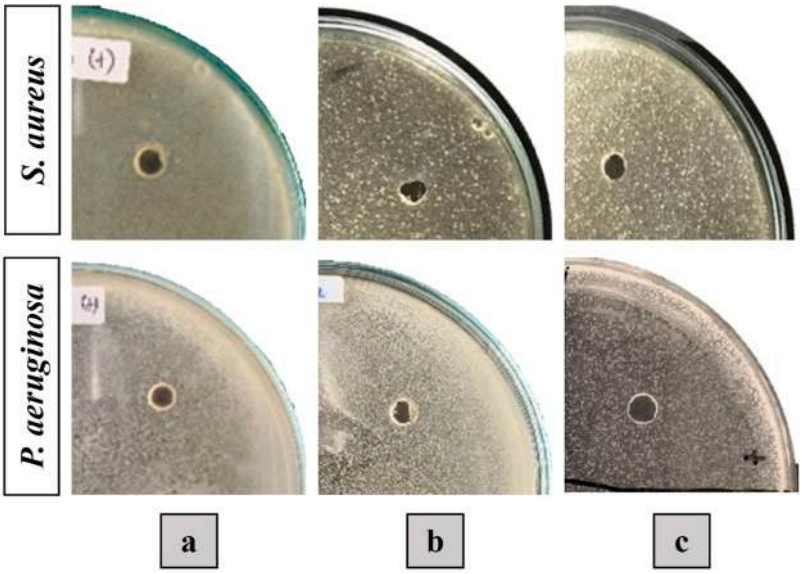

Fig. 11. The antibacterial activity test of commercially available hand gel sanitizers containing 70 % alcohol (a and b), and alcohol 70 % (c).

Table 4
Studies on various bioreductors for the biosynthesis of AgNPs as antibacterial agents.

No	Bioreductor of AgNPs	Inhibition Zones (mm)		Ref.
		S. aureus	*P. aeruginosa*	
1.	Honey	15.92 ± 0.23	15.45 ± 0.88	This work
2.	*Syzygium polyanthum*	13.00 ± 1.32	12.00 ± 0.50	[71]
3.	*Aloe vera*	14.3 ± 0.6	13.1 ± 0.4	[72]
4.	*Arthrospira platensis*	14 ± 0.4	12 ± 0.2	[73]
5.	*Trigonella foenum-graecum*	–	11.26 ± 0.51	[74]
6.	*Acacia nilotica*	12	–	[75]
7.	*Hypsizygus ulmarius*	4.1 ± 0.2	2.1 ± 0.1	[76]
8.	*Persea americana*	–	5.25 ± 0.35	[77]
9.	*Aquilegia pubiflora*	–	9.1 ± 0.34	[78]
10.	*Aristolochia bracteolata*	15.00 ± 0.0	14.66 ± 0.6	[79]

A. bracteolata exhibited comparable activity, with an inhibition zone of 15.00 ± 0.0 mm. Similarly, against *P. aeruginosa*, honey-derived AgNPs achieved the highest inhibition zone of 15.45 ± 0.88 mm, surpassing *S. polyanthum* (12.00 ± 0.50 mm), *A. vera* (13.1 ± 0.4 mm), and *A. platensis* (12 ± 0.2 mm), as well as demonstrating superior activity compared to *H. ulmarius* (2.1 ± 0.1 mm) and *P. americana* (5.25 ± 0.35 mm). The exceptional antibacterial performance of honey-based AgNPs is likely attributed to the unique bioactive components in honey, such as flavonoids, phenols, and enzymes, which enhance nanoparticle reduction and stabilization, resulting in AgNPs with higher antibacterial efficacy. These findings establish honey as a highly effective bioreductant for AgNP synthesis, offering a promising approach to developing advanced antimicrobial solutions, particularly in addressing the critical challenge of antimicrobial resistance [37].

The inhibition zones of AgNPs-Chitosan against *S. aureus* were measured for various honey bioreductors, yielding values of 30.14 ± 0.85 mm for cottonwood, 27.22 ± 1.60 mm for rambutan, 26.61 ± 1.21 mm for rubber, and 26.30 ± 1.56 mm for coffee. For *P. aeruginosa*, the inhibition zones were 21.11 ± 0.36 mm, 20.77 ± 1.40 mm, 20.67 ± 0.58 mm, and 19.85 ± 0.83 mm, respectively. These results diverged slightly from the trends observed with uncoated AgNPs, where the smaller particle size of AgNPs synthesized with coffee honey bioreductor (7.14 nm) demonstrated superior antibacterial activity compared to the larger AgNPs produced with cottonwood honey (11.71 nm). In contrast, the AgNPs-Chitosan revealed that larger particle sizes were associated with enhanced inhibition zones. This phenomenon can be attributed to the increased coating of larger AgNPs with chitosan molecules, which possess inherent antibacterial properties. The synergistic effects of the chitosan coating and the AgNPs likely contribute to the improved antibacterial efficacy observed.

The inhibition zone measurements presented in Table 3 indicate that AgNPs-Chitosan exhibit significantly greater antibacterial activity against Gram-positive bacteria, specifically *S. aureus*, compared to Gram-negative bacteria, such as *P. aeruginosa*. This observation contrasts with the general expectation that Gram-negative bacteria are more susceptible to damage from chitosan, which disrupts cell wall integrity. The fundamental structural differences between Gram-positive and Gram-negative bacteria contribute to this outcome. Gram-positive bacteria possess a thick peptidoglycan layer in their cell wall, while Gram-negative bacteria have a more complex structure characterized by lipopolysaccharides within two membranes [53].

In this research, chitosan was utilized as a coating for AgNPs in the form of very low molecular weight of chitosan (oligochitosan), which is produced through the depolymerization of LMW chitosan. This process involved breaking the glycosidic bonds using hydrogen peroxide (H_2O_2) to generate oligochitosan. The antibacterial mechanism of oligochitosan (molecular weight < 5 kDa) involves both extracellular and intracellular disruption, impacting RNA/DNA integrity, protein synthesis, and mitochondrial function [50,53]. Due to its very low molecular weight, oligochitosan is more adept at passive penetration of the bacterial cell wall, thereby effectively impairing bacterial metabolism.

The hand gel sanitizer formulation containing 10 % AgNPs-Chitosan exhibited antibacterial activity, with inhibition zones ranging from 12.24 mm to 14.48 mm against *S. aureus* and from 13.94 mm to 15.45 mm against *P. aeruginosa*. However, the inhibition zone data did not reveal a consistent trend with respect to the variation in honey bioreductors used. This inconsistency is likely due to the relatively low concentration of AgNPs-Chitosan (10 %), which may have limited the capacity to more thoroughly assess the influence of individual formulation components on antibacterial efficacy. Nevertheless, the AgNPs-Chitosan-based hand gel sanitizer demonstrated superior antibacterial performance compared to the positive control (commercial 70 % alcohol-based hand gel sanitizer) which exhibited only minimal antibacterial activity. These findings suggest that, despite the lower concentration (10 %) of AgNPs-Chitosan, the formulation is more effective in inhibiting bacterial growth than hand gel sanitizers relying solely on alcohol as the antimicrobial agent.

To validate the antibacterial efficacy of commercial hand gel sanitizers containing 70 % alcohol, tests were conducted on two different brands of alcohol-based hand gel sanitizers as well as pure 70 % alcohol (Fig. 11). In this result, neither the alcohol-based hand gel sanitizers nor the pure alcohol demonstrated antibacterial activity against *S. aureus* or *P. aeruginosa*. Our study not only demonstrates that the AgNPs-chitosan-based hand gel sanitizer developed in this work is effective as an antibacterial agent, but also highlights that alcohol-based hand sanitizers are less effective in comparison. However, a limitation of this work is that it does not investigate the underlying reasons for the ineffectiveness of 70 %-alcohol-based hand gel sanitizers as antibacterial agents, nor does it explore biofilm formation in bacterial strains in detail. This is because the primary focus of our work is on developing and thoroughly testing a new hand gel sanitizer formulation that has been proven effective against bacteria. Previous studies [80–86] may have partly addressed these issues.

The reduced efficacy of alcohol-based sanitizers can be attributed to several underlying factors. One significant mechanism involves the formation of biofilms, especially by bacteria such as *S. aureus* [80,81]. Biofilms are structured clusters of bacteria embedded in an extracellular matrix, creating a physical barrier that prevents disinfectants, including alcohol, from effectively penetrating and reaching the bacterial cells. This barrier significantly reduces the antimicrobial action of alcohol, allowing the bacteria within the biofilm to remain protected and viable [82]. In addition, research has shown that alcohol concentrations, such as 70 %, can inadvertently promote the formation of biofilms. This phenomenon occurs because alcohol, while effective in killing planktonic (free-floating) bacteria, may induce a stress response in bacterial cells, leading to enhanced biofilm production as a survival mechanism. As a result, this biofilm formation further hinders the bactericidal efficacy of alcohol, making it less effective against biofilm-forming bacteria [83].

Secondly, the antibacterial activity of alcohol depends on its ability to disrupt bacterial cell membranes and denature proteins. However, in the presence of biofilms or when contact between the alcohol and bacteria is insufficient, this process becomes less effective, resulting in a failure to achieve bactericidal outcomes [84]. Salvage et al. [85] reported that lower alcohol concentrations can sometimes be more effective than 70 %, as they may penetrate bacterial membranes more efficiently without triggering biofilm formation. Optimal antibacterial activity has been observed at concentrations ranging from 37 % to 46 % for *P. aeruginosa* and 42 % to

50 % for *S. aureus*.

Although bacterial resistance to alcohol is uncommon, prolonged exposure to sub-lethal alcohol concentrations can lead to adaptations that increase bacterial tolerance to disinfectants [86]. This suggests that using 70 % alcohol as a standard disinfectant may not be fully effective, and reducing the concentration to a range of 40 % to 50 % could enhance antibacterial effectiveness against certain pathogens [85]. However, resistance to alcohol may still develop through mutations in carbohydrate metabolism and the formation of biofilms, which help bacteria resist alcohol's effects. Biofilms create a protective shield, while metabolic mutations allow bacteria to adapt and survive in high-alcohol environments, further diminishing the bactericidal potency of alcohol-based sanitizers [86].

As a more efficient alternative, AgNPs-Chitosan-based hand gel sanitizers have been proposed as a non-alcohol solution. AgNPs exhibit potent antimicrobial activity through multiple mechanisms, including the release of silver ions that disrupt bacterial cell membranes, interactions with bacterial DNA, and the generation of reactive oxygen species (ROS) that lead to cell death [87,88]. Chitosan, on the other hand, acts as a biofilm-binding agent and enhances antimicrobial efficacy by increasing bacterial cell wall permeability [89,90]. The combination of AgNPs and chitosan offers a more stable and effective approach against pathogens, particularly biofilm-forming and alcohol-tolerant bacteria, such as *S. aureus* and *P. aeruginosa*. This AgNP-Chitosan-based hand gel sanitizer not only addresses bacterial resistance to alcohol but also provides broader protection through its multifaceted mechanisms, inhibiting biofilm formation and disrupting bacterial cell structures.

The antibacterial efficacy of AgNPs-Chitosan-based hand gel sanitizer was assessed after 5 and 20 days of storage at room temperature. The results indicated no significant difference in antibacterial effectiveness over time (Fig. 12**,** Table 5). The inhibition zone of the AgNPs-Chitosan-based hand gel sanitizer after 5 days of storage ranged from 12.95 ± 0.88 mm to 13.43 ± 0.23 mm for *S. aureus* and from 10.31 ± 0.05 mm to 11.43 ± 0.23 mm for *P. aeruginosa*. After 20 days of storage, the inhibition zone increased to 13.60 ± 0.26 mm to 13.98 ± 0.68 mm for *S. aureus* and from 14.12 ± 0.78 mm to 15.01 ± 1.04 mm for *P. aeruginosa*. These findings suggest that the antibacterial activity of the AgNPs-Chitosan-based hand gel sanitizer remains stable after 20 days of storage, with a slight increase in antibacterial efficacy, although not statistically significant.

This enhancement could be attributed to structural changes in the gel matrix during storage, which may affect the distribution of AgNPs and other active ingredients in the formulation. Changes in gel viscosity or network density could improve the formulation's adhesion to the skin, thereby enhancing its antibacterial effectiveness. Additionally, the evaporation of solvent during storage may lead to an increased concentration of AgNPs-Chitosan in the hand gel sanitizer. The rise in AgNP concentration or gel viscosity likely contributes to the observed increase in antibacterial activity.

3.3.4. In vivo toxicity and irritation test

The toxicity test of shrimp larvae exposed to AgNPs-Chitosan-based hand gel sanitizers, reduced with various types of honey, revealed significant differences in toxicity levels. Among the honey types tested, cottonwood honey produced AgNPs with the lowest toxicity, as evidenced by the highest LC_{50} value of 2648.97 ppm (Table 6). Larval mortality increased from 10 % at 1 ppm to 43.33 % at 1000 ppm, demonstrating that cottonwood honey generated more stable AgNPs, with a better chitosan coating effect, leading to a safer and less toxic formulation suitable for use in hand gel sanitizer.

In contrast, the AgNPs-Chitosan-based hand gel sanitizer reduced with rambutan honey exhibited the highest toxicity, with an LC_{50} value of 1339.63 ppm. Mortality rates increased from 6.67 % at 1 ppm to 43.33 % at 1000 ppm, likely due to the bioactive compounds in Rambutan Honey, which produced more reactive AgNPs that did not interact well with the chitosan coating. This resulted in less stable AgNPs, increasing their toxicity, though still within safe levels.

AgNPs-Chitosan-based hand gel sanitizer reduced with rubber honey showed an LC_{50} value of 1834.71 ppm. Larval mortality increased from 10 % at 1 ppm to 46.67 % at 1000 ppm, placing it between cottonwood and rambutan honey in terms of toxicity. Meanwhile, the AgNPs-Chitosan-based hand gel sanitizer reduced with coffee honey had a slightly lower LC_{50} value of 1671.22 ppm compared to the rubber honey formulation. Larval mortality ranged from 3.33 % at 1 ppm to 43.33 % at 1000 ppm.

The toxicity results obtained from the shrimp larvae mortality assay revealed that, despite varying toxicity levels of AgNPs reduced with different types of honey, all samples fell within the LC_{50} range considered safe (>1000 ppm) [91]. In this study, AgNPs-Chitosan, used as a formulation in hand gel sanitizer at a concentration of only 10 %, exhibited beneficial antibacterial effects without causing significant toxic impacts on aquatic organisms.

The results of the primary skin irritation test (in vivo), conducted on adult female Australian rabbits, are presented in Fig. 13. Over a 72-hour observation period, no signs of visible irritation, such as erythema or edema, were detected on the rabbits' skin. These findings suggest that the AgNPs-Chitosan-based hand gel sanitizer does not release any irritants or harmful substances capable of inducing skin irritation. Throughout the entire observation period, the skin of the rabbits remained unaffected, exhibiting no redness, swelling, or signs of discomfort. In fact, the skin appeared to be smoother and visibly cleaner, as illustrated in Fig. 13. This can be attributed to the formulation's use of non-toxic and skin-friendly ingredients, coupled with the potential beneficial effects of honey. Honey is well-known for its anti-inflammatory, antimicrobial, and moisturizing properties, which may have played a role in soothing the skin and enhancing its overall appearance and condition during the study. The absence of irritation, along with the observed improvement in skin texture and appearance, supports the conclusion that the AgNPs-Chitosan-based hand gel sanitizer formulation is safe for topical use and may offer additional dermatological benefits.

3.4. Antibacterial mechanism of AgNPs-Chitosan

While the exact mechanisms underlying the antibacterial properties of AgNPs remain incompletely understood, their multifaceted

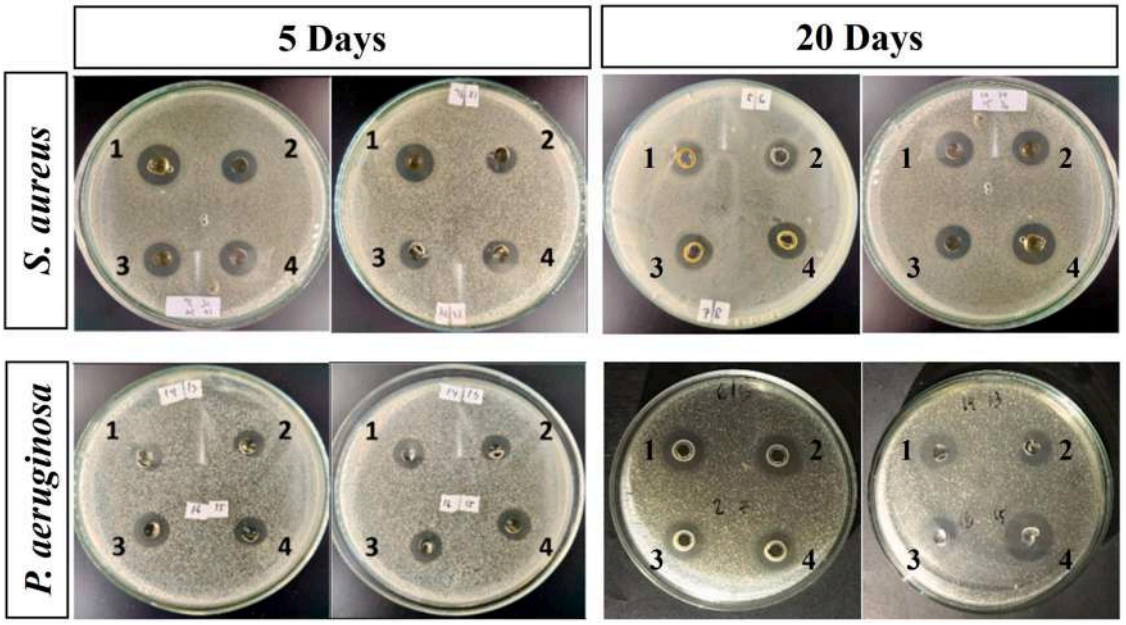

Fig. 12. Antibacterial effectiveness test of AgNPs-Chitosan-based hand gel sanitizer product after 5 days and 20 days of storage.

Table 5
Antibacterial activity test results of AgNPs-Chitosan-based hand gel sanitizer (after 5 and 20 days of storage).

Code	Sample Type		Inhibition Zones (mm)	
			S. aureus	*P. aeruginosa*
1	Hand gel sanitizer based AgNPs-Chitosan (5 Days)	Cottonwood	14.81 ± 0.54	13.31 ± 0.05
2		Rambutan	12.24 ± 1.03	13.43 ± 0.23
3		Rubber	13.84 ± 0.94	13.28 ± 1.17
4		Coffee	14.14 ± 0.69	12.95 ± 0.88
1	Hand gel sanitizer based AgNPs-Chitosan (20 Days)	Cottonwood	13.98 ± 0.68	14.56 ± 0.66
2		Rambutan	13.60 ± 0.26	14.12 ± 0.78
3		Rubber	13.87 ± 0.24	14.67 ± 0.71
4		Coffee	13.94 ± 0.31	15.01 ± 1.04

Table 6
Toxicity evaluation of AgNPs-Chitosan-based hand gel sanitizer on brine shrimp larvae with different AgNPs reducing agents.

Bioreductor of AgNPs	Concentration (ppm)	Number of Surviving Nauplii (24 h)			Total of Nauplii Survivors	% Mortality	LC_{50} (ppm)
		T1	T2	T3			
Cottonwood Honey	1	8	10	9	27	10.00	2648.97
	10	7	8	9	24	20.00	
	100	8	7	6	21	30.00	
	1000	6	6	5	17	43.33	
Rambutan Honey	1	9	10	9	28	6.67	1339.63
	10	7	8	8	23	23.33	
	100	7	7	6	20	33.33	
	1000	5	6	6	17	43.33	
Rubber Honey	1	10	8	9	27	10.00	1834.71
	10	9	7	8	24	20.00	
	100	7	8	6	21	30.00	
	1000	5	5	6	16	46.67	
Coffee Honey	1	10	10	9	29	3.33	1671.22
	10	9	9	8	26	13.33	
	100	7	8	7	22	26.67	
	1000	5	6	6	17	43.33	

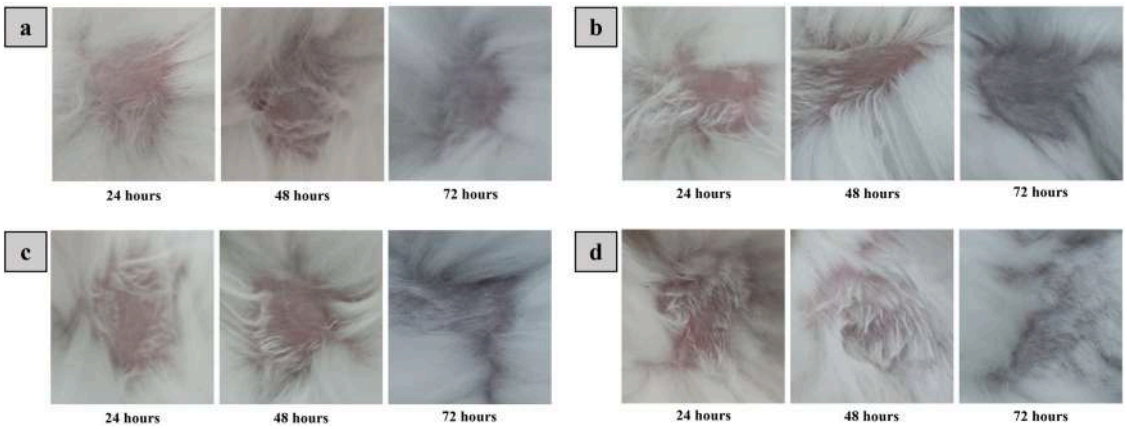

Fig. 13. Primary irritation test results of AgNPs-Chitosan based hand gel sanitizer with cottonwood (a), rambutan (b), rubber (c) and coffee (d) honey bioreductors on adult female autralian rabbits for 24, 48, and 72 h.

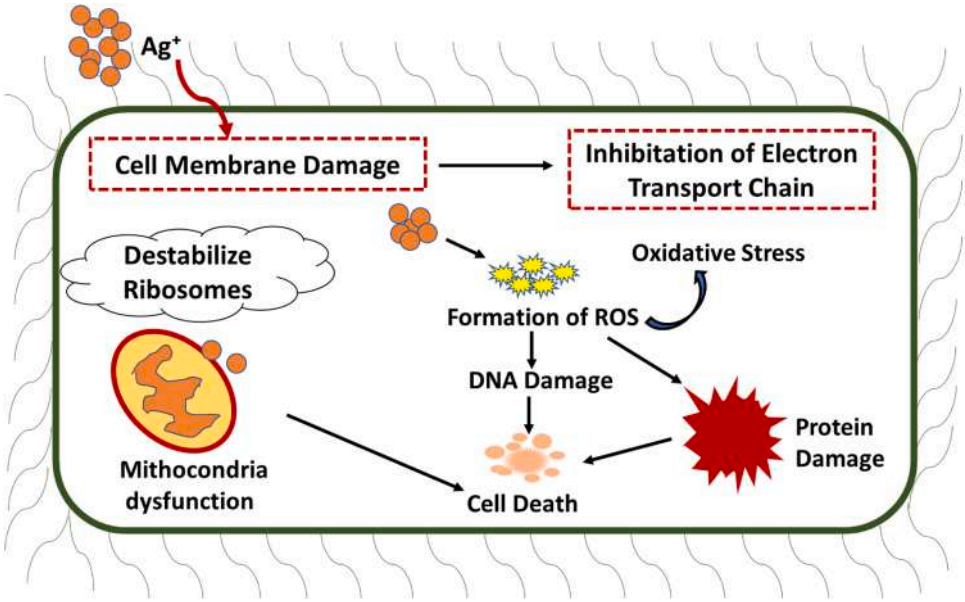

Fig. 14. Antibacterial mechanism of AgNPs.

antibacterial actions are illustrated in Fig. 14. AgNPs operate as antibacterial agents through a complex mode of action. They release silver ions (Ag^{+}), which adhere to bacterial cell walls and cytoplasmic membranes via electrostatic interactions with sulfur-containing proteins. This binding enhances membrane permeability, resulting in the leakage of cellular contents. Furthermore, silver ions inhibit the electron transport chain, leading to a reduction in adenosine triphosphate (ATP) production and subsequent metabolic dysfunction. AgNPs also promote the generation of reactive oxygen species (ROS), highly reactive molecules that can inflict damage on critical cellular components, including DNA, proteins, and lipids, thereby inducing oxidative stress and additional cellular injury. The interaction of silver ions with sulfur and phosphorus in DNA can hinder bacterial DNA replication and cell division. Additionally, AgNPs may induce ribosomal denaturation, disrupting the synthesis of essential proteins, ultimately culminating in bacterial cell death. Beyond the release of silver ions, AgNPs can accumulate in the depressions of the bacterial cell wall, further exacerbating structural damage and contributing to cell death. Collectively, these mechanisms elucidate the efficacy of AgNPs in inhibiting bacterial growth and inducing cell death [19].

The antibacterial activity of AgNPs-Chitosan of honey is attributed to a combination of synergistic mechanisms that disrupt bacterial integrity and hinder their survival. One key mechanism is the disruption of the bacterial cell membrane. AgNPs-Chitosan interact with the negatively charged components of the bacterial cell wall, compromising the membrane's integrity. This disruption increases membrane permeability, leading to the leakage of intracellular contents and ultimately resulting in bacterial cell death. Scanning electron microscopy studies have visually confirmed this membrane-damaging effect caused by AgNPs-Chitosan [92].

The polycationic nature of chitosan enhances antibacterial activity through electrostatic interactions. In acidic environments, where chitosan becomes protonated, it binds more effectively to the anionic surfaces of bacterial cells. This increased binding affinity disrupts bacterial cellular functions, further strengthening the antimicrobial effect of AgNPs-Chitosan. Another critical antibacterial mechanism involves DNA binding and replication inhibition. Chitosan can bind directly to bacterial DNA, interfering with replication processes. This action inhibits bacterial growth and reproduction, contributing significantly to the bactericidal effect [90].

Additionally, chitosan exhibits chelating properties, allowing it to bind to trace metal ions essential for bacterial growth. By depriving bacteria of these vital nutrients, chitosan disrupts their metabolic functions, which can lead to toxic effects within the bacterial cells. Together, these combined mechanisms highlight the effectiveness of AgNPs-Chitosan as a potent antibacterial agent. The synergistic interaction between AgNPs and chitosan enables the compound to target bacterial cells through multiple pathways, making it highly effective in combating bacterial infections [90,92].

4. Conclusions

The study demonstrates that AgNPs, synthesized using honey as a bioreductant and coated with oligochitosan, possess significant potential as a sustainable antimicrobial agent. *C. pentandra* honey produced AgNPs with an average particle size of 11.71 nm, exhibiting enhanced antibacterial efficacy, particularly after oligochitosan coating. The AgNPs-Chitosan-based hand gel sanitizer formulation, characterized by stable pH values (4.0–4.3) and high resistance to syneresis at 5 °C and 40 °C, displayed superior antibacterial activity compared to alcohol-based hand gel sanitizers, with inhibition zones against *S. aureus* and *P. aeruginosa* measuring 14.84 ± 0.4 mm and 11.16 ± 0.73 mm, respectively. Dermatological assessments confirmed its safety, showing no skin irritation after 72 h of application. Furthermore, toxicity evaluations revealed low toxicity, with the highest LC_{50} value (2648.97 ppm) observed for AgNPs derived from *C. pentandra* honey. Combining stability, antibacterial performance, and safety, this formulation highlights the potential of AgNPs-Chitosan as an innovative and sustainable antimicrobial solution to address the global challenge of antimicrobial resistance.

Declaration of generative AI and AI-assisted technologies in the writing process

During the preparation of this work, the authors used ChatGPT to enhance the readability of the English language.

Data statement

All data related to this article are included in this paper.

CRediT authorship contribution statement

Saidun Fiddaroini: Writing – review & editing, Writing – original draft, Visualization, Software, Investigation, Formal analysis. **Kurnia Indu:** Investigation, Formal analysis. **Luailik Madaniyah:** Writing – review & editing, Writing – original draft, Visualization. **Suci Amalia:** Supervision, Investigation, Conceptualization. **Aulanni'am:** Funding acquisition, Conceptualization. **Moh. Farid Rahman:** Methodology, Investigation, Conceptualization. **Akhmad Sabarudin:** Methodology, Investigation, Funding acquisition, Conceptualization.

Declaration of competing interest

The authors declare that they have no known competing financial interests or personal relationships that could have appeared to influence the work reported in this paper.

Acknowledgements

The authors would like to thank the Faculty of Science, Brawijaya University through the financial support through the Professorship Grant, with the number: 02172.6/UN10.F0901/B/KS/2024.

References

[1] C.J. Murray, K.S. Ikuta, F. Sharara, L. Swetschinski, G. Robles Aguilar, A. Gray, M. Naghavi, Global burden of bacterial antimicrobial resistance in 2019: a systematic analysis, The Lancet 399 (10325) (2022) 629–655, https://doi.org/10.1016/S0140-6736(21)02724-0.

[2] Samreen, I. Ahmad, H.A. Malak, H.H Abulreesh, Environmental antimicrobial resistance and its drivers: a potential threat to public health, J. Glob. Antimicrob. Resist. 27 (2021) 101–111, https://doi.org/10.1016/j.jgar.2021.08.001.

[3] Md.A. Salam, Md.Y. Al-Amin, M.T. Salam, J.S. Pawar, N. Akhter, A.A. Rabaan, M.A.A. Alqumber, Antimicrobial resistance: a growing serious threat for global public health, Healthcare 11 (13) (2023) 1946, https://doi.org/10.3390/healthcare11131946.

[4] G. Muteeb, M.T. Rehman, M. Shahwan, M. Aatif, Origin of antibiotics and antibiotic resistance, and their impacts on drug development: a narrative review, Pharmaceuticals 16 (11) (2023) 1615, https://doi.org/10.3390/ph16111615.

[5] N. Rabiee, M. Bagherzadeh, M. Tavakolizadeh, A. Pourjavadi, M. Atarod, T.J. Webster, Synthesis, characterization and mechanistic study of nano chitosan tetrazole as a novel and promising platform for CRISPR delivery, Int. J. Polym. Mater. Polymeric Biomater. 71 (2) (2022) 116–126, https://doi.org/10.1080/00914037.2020.1809405.

[6] T. Bruna, F. Maldonado-Bravo, P. Jara, N. Caro, Silver nanoparticles and their antibacterial applications, Int. J. Mol. Sci. 22 (13) (2021) 7202, https://doi.org/10.3390/ijms22137202.

[7] E. Urnukhsaikhan, B.-E. Bold, A. Gunbileg, N. Sukhbaatar, T. Mishig-Ochir, Antibacterial activity and characteristics of silver nanoparticles biosynthesized from Carduus crispus, Sci. Rep. 11 (1) (2021) 21047, https://doi.org/10.1038/s41598-021-00520-2.

[8] Hemlata, P.R. Meena, A.P. Singh, K.K Tejavath, Biosynthesis of silver nanoparticles using *Cucumis prophetarum* aqueous leaf extract and their antibacterial and antiproliferative activity against cancer cell lines, ACS. Omega 5 (10) (2020) 5520–5528, https://doi.org/10.1021/acsomega.0c00155.

[9] A. Rautela, J. Rani, M. Debnath (Das), Green synthesis of silver nanoparticles from Tectona grandis seeds extract: characterization and mechanism of antimicrobial action on different microorganisms, J. Anal. Sci. Technol. 10 (1) (2019) 5, https://doi.org/10.1186/s40543-018-0163-z.

[10] C. Vanlalveni, S. Lallianrawna, A. Biswas, M. Selvaraj, B. Changmai, S.L. Rokhum, Green synthesis of silver nanoparticles using plant extracts and their antimicrobial activities: a review of recent literature, RSC. Adv. 11 (5) (2021) 2804–2837, https://doi.org/10.1039/D0RA09941D.

[11] M.G. Toudeshkchoui, N. Rabiee, M. Rabiee, M. Bagherzadeh, M. Tahriri, L. Tayebi, M.R. Hamblin, Microfluidic devices with gold thin film channels for chemical and biomedical applications: a review, Biomed. MicroDevices 21 (4) (2019) 93, https://doi.org/10.1007/s10544-019-0439-0.

[12] K. Markowska, A.M. Grudniak, K.I. Wolska, Silver nanoparticles as an alternative strategy against bacterial biofilms, Acta Biochim. Pol. 60 (4) (1970), https://doi.org/10.18388/abp.2013_2016.

[13] N. Rabiee, M. Bagherzadeh, A.M. Ghadiri, Y. Fatahi, A. Aldhaher, P. Makvandi, R.S. Varma, Turning toxic Nanomaterials into a safe and bioactive Nanocarrier for Co-delivery of DOX/pCRISPR, ACS. Appl. Bio Mater. 4 (6) (2021) 5336–5351, https://doi.org/10.1021/acsabm.1c00447.

[14] Z.A. Ratan, M.F. Haidere, Md. Nurunnabi, S.Md. Shahriar, A.J.S. Ahammad, Y.Y. Shim, J.Y. Cho, Green chemistry synthesis of silver nanoparticles and their potential anticancer effects, Cancers. (Basel) 12 (4) (2020) 855, https://doi.org/10.3390/cancers12040855.

[15] A. Dhaka, S. Chand Mali, S. Sharma, R. Trivedi, A review on biological synthesis of silver nanoparticles and their potential applications, Results. Chem. 6 (2023) 101108, https://doi.org/10.1016/j.rechem.2023.101108.

[16] G. Czernel, D. Bloch, A. Matwijczuk, J. Cieśla, M. Kędzierska-Matysek, M. Florek, M. Gagoś, Biodirected synthesis of silver nanoparticles using aqueous honey solutions and evaluation of their antifungal activity against pathogenic Candida Spp, Int. J. Mol. Sci. 22 (14) (2021) 7715, https://doi.org/10.3390/ijms22147715.

[17] M. Sarvepalli, A. Velidandi, N. Korrapati, Chemical vs biological silver nanoparticles: synthesis, characterization, properties, and in vitro applications, Inorg. Chem. Commun. 167 (2024) 112667, https://doi.org/10.1016/j.inoche.2024.112667.

[18] U.T. Khatoon, A. Velidandi, G.V.S. Nageswara Rao, Copper oxide nanoparticles: synthesis via chemical reduction, characterization, antibacterial activity, and possible mechanism involved, Inorg. Chem. Commun. 149 (2023) 110372, https://doi.org/10.1016/j.inoche.2022.110372.

[19] I.X. Yin, J. Zhang, I.S. Zhao, M.L. Mei, Q. Li, C.H. Chu, The antibacterial mechanism of silver nanoparticles and its application in dentistry, Int. J. Nanomedicine 15 (2020) 2555–2562, https://doi.org/10.2147/IJN.S246764.

[20] S. Fiddaroini, K. Indu, S. Amalia, I.O. Wulandari, A. Mulyasuryani, L. Dinira, A. Sabarudin, Cottonwood honey (Ceiba pentandra) as Bioreductor for preparation of AgNPs-mediated chitosan-based hand gel sanitizer, Trop. J. Natural Product Res. 7 (12) (2023), https://doi.org/10.26538/tjnpr/v7i12.29.

[21] G. Bonsignore, M. Patrone, S. Martinotti, E. Ranzato, Green" biomaterials: the promising role of honey, J. Funct. Biomater. 12 (4) (2021) 72, https://doi.org/10.3390/jfb12040072.

[22] C.P. Jiménez-Gómez, J.A. Cecilia, Chitosan: a natural biopolymer with a wide and varied range of applications, Molecules. 25 (17) (2020) 3981, https://doi.org/10.3390/molecules25173981.

[23] S. Zhang, M. Ali, F. Nawaz, N. Ali, A. Khan, F. Ali, T. Al-Harthy, Scaffolds of Chitosan-metallic hybrids as antimicrobial wound dressing, J. Mol. Liq. (2024) 126541, https://doi.org/10.1016/j.molliq.2024.126541.

[24] E. Mirda, R. Idroes, K. Khairan, T.E. Tallei, M. Ramli, N. Earlia, Z. Jalil, Synthesis of chitosan-silver nanoparticle composite spheres and their antimicrobial activities, Polymers. (Basel) 13 (22) (2021) 3990, https://doi.org/10.3390/polym13223990.

[25] M. Ul-Islam, K.F. Alabbosh, S. Manan, S. Khan, F. Ahmad, M.W. Ullah, Chitosan-based nanostructured biomaterials: synthesis, properties, and biomedical applications, Adv. Ind. Eng. Polym. Res. 7 (1) (2024) 79–99, https://doi.org/10.1016/j.aiepr.2023.07.002.

[26] S. Mumtaz, S. Ali, S. Mumtaz, T.A. Mughal, H.M. Tahir, H.A. Shakir, Chitosan conjugated silver nanoparticles: the versatile antibacterial agents, Polym. Bull. 80 (5) (2023) 4719–4736, https://doi.org/10.1007/s00289-022-04321-z.

[27] L. Madaniyah, S. Fiddaroini, E.K. Hayati, Moh.F. Rahman, A. Sabarudin, Biosynthesis, characterization, and in-vitro anticancer effect of plant-mediated silver nanoparticles using Acalypha indica Linn: in-silico approach, OpenNano 21 (2025) 100220, https://doi.org/10.1016/j.onano.2024.100220.

[28] H.A. Ghramh, S.A. Alrumman, I. Ahmad, A. Kalam, S.E.I. Elbehairi, A.M. Alfaify, K.A. Khan, Chemical characterization of honey and its effect (Alone as well as with Synthesized Silver Nanoparticles) on microbial pathogens' and human cancer cell lines' Growth, Nutrients. 15 (3) (2023) 684, https://doi.org/10.3390/nu15030684.

[29] S. Al-Musawi, S. Albukhaty, H. Al-Karagoly, G.M. Sulaiman, M.S. Alwahibi, Y.H. Dewir, H. Rizwana, Antibacterial activity of Honey/Chitosan nanofibers loaded with capsaicin and gold nanoparticles for wound dressing, Molecules. 25 (20) (2020) 4770, https://doi.org/10.3390/molecules25204770.

[30] I.O. Wulandari, B.E. Pebriatin, V. Valiana, S. Hadisaputra, A.D. Ananto, A. Sabarudin, Green synthesis of silver nanoparticles coated by water soluble chitosan and its potency as non-alcoholic hand sanitizer formulation, Materials 15 (13) (2022) 4641, https://doi.org/10.3390/ma15134641.

[31] P. Prajapati, H. Desai, C. Chandarana, Hand sanitizers as a preventive measure in COVID-19 pandemic, its characteristics, and harmful effects: a review, J. Egypt. Public Health Assoc. 97 (1) (2022) 6, https://doi.org/10.1186/s42506-021-00094-x.

[32] Z.B. Nqakala, N.R.S. Sibuyi, A.O. Fadaka, M. Meyer, M.O. Onani, A.M. Madiehe, Advances in nanotechnology towards development of silver nanoparticle-based wound-healing agents, Int. J. Mol. Sci. 22 (20) (2021) 11272, https://doi.org/10.3390/ijms222011272.

[33] S.M. Mawazi, M. Kumar, N. Ahmad, Y. Ge, S. Mahmood, Recent applications of chitosan and its derivatives in antibacterial, anticancer, wound healing, and tissue engineering fields, Polymers. (Basel) 16 (10) (2024) 1351, https://doi.org/10.3390/polym16101351.

[34] A.P. Golin, D. Choi, A. Ghahary, Hand sanitizers: a review of ingredients, mechanisms of action, modes of delivery, and efficacy against coronaviruses, Am. J. Infect. Control 48 (9) (2020) 1062–1067, https://doi.org/10.1016/j.ajic.2020.06.182.

[35] R.Y. Booq, A.A. Alshehri, F.A. Almughem, N.M. Zaidan, W.S. Aburayan, A.A. Bakr, E.A. Tawfik, Formulation and evaluation of alcohol-free hand sanitizer gels to prevent the spread of infections during pandemics, Int. J. Environ. Res. Public Health 18 (12) (2021) 6252, https://doi.org/10.3390/ijerph18126252.

[36] A.S. Kumar, G. Madhu, E. John, S.V. Kuttinarayanan, S.K. Nair, Optical and antimicrobial properties of silver nanoparticles synthesized via green route using honey, Green Process. Synthesis 9 (1) (2020) 268–274, https://doi.org/10.1515/gps-2020-0029.

[37] G. Czernel, D. Bloch, A. Matwijczuk, J. Cieśla, M. Kędzierska-Matysek, M. Florek, M. Gagoś, Biodirected synthesis of silver nanoparticles using aqueous honey solutions and evaluation of their antifungal activity against pathogenic Candida Spp, Int. J. Mol. Sci. 22 (14) (2021) 7715, https://doi.org/10.3390/ijms22147715.

[38] G. Assylbekova, H.F. Alotaibi, S. Yegemberdiyeva, A. Suigenbayeva, M. Sataev, S. Koshkarbaeva, P. Prokopovich, Sunlight induced synthesis of silver nanoparticles on cellulose for the preparation of antimicrobial textiles, J. Photochem. Photobiol. 11 (2022) 100134, https://doi.org/10.1016/j.jpap.2022.100134.

[39] H. Rizwana, M.S. Alwhibi, R.A. Al-Judaie, H.A. Aldehaish, N.S. Alsaggabi, Sunlight-mediated green synthesis of silver nanoparticles using the berries of Ribes rubrum (Red Currants): characterisation and evaluation of their antifungal and antibacterial activities, Molecules. 27 (7) (2022) 2186, https://doi.org/10.3390/molecules27072186.

[40] V. Kumar, D.K. Singh, S. Mohan, R.K. Gundampati, S.H. Hasan, Photoinduced green synthesis of silver nanoparticles using aqueous extract of Physalis angulata and its antibacterial and antioxidant activity, J. Environ. Chem. Eng. 5 (1) (2017) 744–756, https://doi.org/10.1016/j.jece.2016.12.055.

[41] M. Jayapriya, D. Dhanasekaran, M. Arulmozhi, E. Nandhakumar, N. Senthilkumar, K. Sureshkumar, Green synthesis of silver nanoparticles using Piper longum catkin extract irradiated by sunlight: antibacterial and catalytic activity, Res. Chem. Intermed. 45 (6) (2019) 3617–3631, https://doi.org/10.1007/s11164-019-03812-5.

[42] J.S. Moodley, S.B.N. Krishna, K. Pillay, Sershen, P Govender, Green synthesis of silver nanoparticles from *Moringa oleifera* leaf extracts and its antimicrobial potential, Adv. Natural Sci.: Nanosci. Nanotechnol. 9 (1) (2018) 015011, https://doi.org/10.1088/2043-6254/aaabb2.
[43] M.K. Indana, B.R. Gangapuram, R. Dadigala, R. Bandi, V. Guttena, A novel green synthesis and characterization of silver nanoparticles using gum tragacanth and evaluation of their potential catalytic reduction activities with methylene blue and Congo red dyes, J. Anal. Sci. Technol. 7 (1) (2016) 19, https://doi.org/10.1186/s40543-016-0098-1.
[44] H. Sun, R. Jiao, G. An, H. Xu, D. Wang, Influence of particle size on the aggregation behavior of nanoparticles: role of structural hydration layer, J. Environ. Sci. 103 (2021) 33–42, https://doi.org/10.1016/j.jes.2020.10.007.
[45] S.S. Al-Zahrani, S.M. Al-Garni, Fabrication of antifungal AgNPs capped with chitosan using endophytic fungus Curvularia kusanoi, Biocatal. Agric. Biotechnol. 51 (2023) 102769, https://doi.org/10.1016/j.bcab.2023.102769.
[46] I. Aranaz, F. Navarro-García, M. Morri, N. Acosta, L. Casettari, A. Heras, Evaluation of chitosan salt properties in the production of AgNPs materials with antibacterial activity, Int. J. Biol. Macromol. 235 (2023) 123849, https://doi.org/10.1016/j.ijbiomac.2023.123849.
[47] A.Z. Hameed, S.A. Raj, J. Kandasamy, M.A. Baghdadi, M.A. Shahzad, Chitosan: a sustainable material for multifarious applications, Polymers. (Basel) 14 (12) (2022) 2335, https://doi.org/10.3390/polym14122335.
[48] T.T.V. Phan, D.T. Phan, X.T. Cao, T.-C. Huynh, J. Oh, Roles of chitosan in green synthesis of metal nanoparticles for biomedical applications, Nanomaterials 11 (2) (2021) 273, https://doi.org/10.3390/nano11020273.
[49] M. Ottonelli, S. Zappia, A. Demartini, M. Alloisio, Chitosan-stabilized noble metal nanoparticles: study of their shape evolution and post-functionalization properties, Nanomaterials 10 (2) (2020) 224, https://doi.org/10.3390/nano10020224.
[50] R. Teixeira-Santos, M. Lima, L.C. Gomes, F.J. Mergulhão, Antimicrobial coatings based on chitosan to prevent implant-associated infections: a systematic review, iScience 24 (12) (2021) 103480, https://doi.org/10.1016/j.isci.2021.103480.
[51] P. Mendez-Pfeiffer, M.G. Ballesteros-Monrreal, J. Juarez, M. Gastelum-Cabrera, P. Martinez-Flores, P. Taboada, D. Valencia, Chitosan-coated silver nanoparticles inhibit adherence and biofilm formation of Uropathogenic *Escherichia coli*, ACS. Infect. Dis. 10 (4) (2024) 1126–1136, https://doi.org/10.1021/acsinfecdis.3c00229.
[52] G.J.C. Canama, M.C.L. Delco, R.A. Talandron, N.P. Tan, Synthesis of chitosan-silver nanocomposite and its evaluation as an antibacterial coating for mobile phone glass protectors, ACS. Omega 8 (20) (2023) 17699–17711, https://doi.org/10.1021/acsomega.3c00191.
[53] C.-L. Ke, F.-S. Deng, C.-Y. Chuang, C.-H. Lin, Antimicrobial actions and applications of Chitosan, Polymers. (Basel) 13 (6) (2021) 904, https://doi.org/10.3390/polym13060904.
[54] P. Rivero-Ramos, M.G. Unthank, T. Sanz, M.D. Rodrigo, M. Benlloch-Tinoco, Synergistic depolymerisation of alginate and chitosan by high hydrostatic pressure (HHP) and pulsed electric fields (PEF) treatment in the presence of H2O2, Carbohydr. Polym. 316 (2023) 120999, https://doi.org/10.1016/j.carbpol.2023.120999.
[55] A. Chamidah, C.N. Widiyanti, N.N. Fabiyani, Utilization of water-soluble chitosan as antiseptic hand sanitizer, J. Perikanan Universitas Gadjah Mada 21 (1) (2019) 9, https://doi.org/10.22146/jfs.38750.
[56] E. Saion, E. Gharibshahi, K. Naghavi, Size-controlled and optical properties of monodispersed silver nanoparticles synthesized by the radiolytic reduction method, Int. J. Mol. Sci. 14 (4) (2013) 7880–7896, https://doi.org/10.3390/ijms14047880.
[57] E.A. Skomorokhova, T.P. Sankova, I.A. Orlov, A.N. Savelev, D.N. Magazenkova, M.G. Pliss, E.Y. Ilyechova, Size-dependent bioactivity of silver nanoparticles: antibacterial properties, influence on copper status in mice, and whole-body turnover, Nanotechnol. Sci. Appl. 13 (2020) 137–157, https://doi.org/10.2147/NSA.S287658.
[58] D. Arif, M.B.K. Niazi, N. Ul-Haq, M.N. Anwar, E. Hashmi, Preparation of antibacterial cotton fabric using chitosan-silver nanoparticles, Fibers Polym. 16 (7) (2015) 1519–1526, https://doi.org/10.1007/s12221-015-5245-6.
[59] D. Yan, Y. Li, Y. Liu, N. Li, X. Zhang, C. Yan, Antimicrobial properties of chitosan and chitosan derivatives in the treatment of enteric infections, Molecules. 26 (23) (2021) 7136, https://doi.org/10.3390/molecules26237136.
[60] L. Cinteza, C. Scomoroscenco, S. Voicu, C. Nistor, S. Nitu, B. Trica, C. Petcu, Chitosan-stabilized Ag nanoparticles with superior biocompatibility and their synergistic antibacterial effect in mixtures with essential oils, Nanomaterials 8 (10) (2018) 826, https://doi.org/10.3390/nano8100826.
[61] S. Ponarulselvam, C. Panneerselvam, K. Murugan, N. Aarthi, K. Kalimuthu, S. Thangamani, Synthesis of silver nanoparticles using leaves of Catharanthus roseus Linn. G. Don and their antiplasmodial activities, Asian Pac. J. Trop. Biomed. 2 (7) (2012) 574–580, https://doi.org/10.1016/S2221-1691(12)60100-2.
[62] W. Handayani, A.S. Ningrum, C. Imawan, The role of pH in synthesis silver nanoparticles using Pometia pinnata (Matoa) leaves extract as Bioreductor, J. Phys.: Conf. Ser. 1428 (1) (2020) 012021, https://doi.org/10.1088/1742-6596/1428/1/012021.
[63] S. Raza, M. Wdowiak, M. Grotek, W. Adamkiewicz, K. Nikiforow, P. Mente, J. Paczesny, Enhancing the antimicrobial activity of silver nanoparticles against ESKAPE bacteria and emerging fungal pathogens by using tea extracts, Nanoscale Adv. 5 (21) (2023) 5786–5798, https://doi.org/10.1039/D3NA00220A.
[64] S.A. Sadat Shandiz, M. Shafiee Ardestani, D. Shahbazzadeh, A. Assadi, R. Ahangari Cohan, V. Asgary, S. Salehi, Novel imatinib-loaded silver nanoparticles for enhanced apoptosis of human breast cancer MCF-7 cells, Artif. Cells Nanomed. Biotechnol. 45 (6) (2017) 1082–1091, https://doi.org/10.1080/21691401.2016.1202257.
[65] M.M. Cavia, M.A. Fernández-Muiño, E. Gömez-Alonso, M.J. Montes-Pérez, J.F. Huidobro, M.T. Sancho, Evolution of fructose and glucose in honey over one year: influence of induced granulation, Food Chem. 78 (2) (2002) 157–161, https://doi.org/10.1016/S0308-8146(01)00393-4.
[66] S.-H. Kuo, C.-J. Shen, C.-F. Shen, C.-M. Cheng, Role of pH value in clinically relevant diagnosis, Diagnostics 10 (2) (2020) 107, https://doi.org/10.3390/diagnostics10020107.
[67] T. Divoux, B. Mao, P. Snabre, Syneresis and delayed detachment in agar plates, Soft. Matter. 11 (18) (2015) 3677–3685, https://doi.org/10.1039/C5SM00433K.
[68] V. Guénard-Lampron, S. Villeneuve, D. St-Gelais, S.L. Turgeon, Relationship between smoothing temperature, storage time, syneresis and rheological properties of stirred yogurt, Int. Dairy. J. 109 (2020) 104742, https://doi.org/10.1016/j.idairyj.2020.104742.
[69] H.-T.V. Lin, J.-S. Tsai, H.-H. Liao, W.-C. Sung, The effect of hydrocolloids on penetration tests and Syneresis of binary gum gels and modified corn Starch–Gum gels, Gels. 9 (8) (2023) 605, https://doi.org/10.3390/gels9080605.
[70] U. Thahira Khatoon, A. Velidandi, G.V.S. Nageswara Rao, Nano-sized copper particles: chemical synthesis, characterization, and their size and surface charge dependent antibacterial potential, Results. Chem. 7 (2024) 101258, https://doi.org/10.1016/j.rechem.2023.101258.
[71] S. Khan, Y. Rukayadi, A.H. Jaafar, N.H. Ahmad, Antibacterial potential of silver nanoparticles (SP-AgNPs) synthesized from Syzygium polyanthum (Wight) Walp. against selected foodborne pathogens, Heliyon. 9 (12) (2023) e22771, https://doi.org/10.1016/j.heliyon.2023.e22771.
[72] A. Ahmed Al-mehdhar, K. Mohammed Alarjani, N. Salem Aldosari, M. Ahmed Alghamdi, Antibacterial efficacy of AgNPs synthesized from extract and staphylococcus aureus culture supernatant, J. King Saud Univ. - Sci. 36 (10) (2024) 103464, https://doi.org/10.1016/j.jksus.2024.103464.
[73] Z.H. Obaid, S.A. Juda, A.F. Kaizal, J. Mohammed Salman, Biosynthesis of silver nano particles (AgNPs) from blue green algae (Arthrospira platensis) and their anti-pathogenic applications, J. King Saud Univ. - Sci. 36 (7) (2024) 103264, https://doi.org/10.1016/j.jksus.2024.103264.
[74] K. Maniah, F. Olyan Al-Otibi, S. Mohamed, B.A. Said, M. Ragab AbdelGawwad, M. Taha Yassin, Synergistic antibacterial activity of biogenic AgNPs with antibiotics against multidrug resistant bacterial strains, J. King Saud Univ. - Sci. 36 (10) (2024) 103461, https://doi.org/10.1016/j.jksus.2024.103461.
[75] S. Revathi, S. Sutikno, A.F. Hasan, A.B. Altemimi, Q.H. ALKaisy, A.J. Phillips, T.G. Abedelmaksoud, Green synthesis and characterization of silver nanoparticles (AgNP) using Acacia nilotica plant extract and their anti-bacterial activity, Food Chem. Adv. 4 (2024) 100680, https://doi.org/10.1016/j.focha.2024.100680.
[76] K. Manimaran, D.H.Y. Yanto, S.H. Anita, O.D. Nurhayat, K. Selvaraj, S. Basavarajappa, K. Kumarasamy, Synthesis and characterization of Hypsizygus ulmarius extract mediated silver nanoparticles (AgNPs) and test their potentiality on antimicrobial and anticancer effects, Environ. Res. 235 (2023) 116671, https://doi.org/10.1016/j.envres.2023.116671.
[77] G. Rajkumar, R. Sundar, Biogenic one-step synthesis of silver nanoparticles (AgNPs) using an aqueous extract of Persea americana seed: characterization, phytochemical screening, antibacterial, antifungal and antioxidant activities, Inorg. Chem. Commun. 143 (2022) 109817, https://doi.org/10.1016/j.inoche.2022.109817.

[78] H. Jan, G. Zaman, H. Usman, R. Ansir, S. Drouet, N. Gigliolo-Guivarc'h, B.H. Abbasi, Biogenically proficient synthesis and characterization of silver nanoparticles (Ag-NPs) employing aqueous extract of Aquilegia pubiflora along with their in vitro antimicrobial, anti-cancer and other biological applications, J. Mater. Res. Technol. 15 (2021) 950–968, https://doi.org/10.1016/j.jmrt.2021.08.048.
[79] A.-T. Le, H.-A. Ha, M.M. Al-Ansari, K. Elankathirselvan, L.A. Al-Humaid, Aristolochia bracteolata flower extract based phytosynthesis and characterization of AgNPs: antimicrobial, antidiabetic, and antioxidant activities potential assessment, Environ. Res. 251 (2024) 118729, https://doi.org/10.1016/j.envres.2024.118729.
[80] M. Bhattacharya, D.J. Wozniak, P. Stoodley, L. Hall-Stoodley, Prevention and treatment of staphylococcus aureus biofilms, Expert. Rev. Anti. Infect. Ther. 13 (12) (2015) 1499–1516, https://doi.org/10.1586/14787210.2015.1100533.
[81] R. Elawady, A.G. Aboulela, A. Gaballah, A.A. Ghazal, A.N. Amer, Antimicrobial Sub-MIC induces Staphylococcus aureus biofilm formation without affecting the bacterial count, BMC. Infect. Dis. 24 (1) (2024) 1065, https://doi.org/10.1186/s12879-024-09790-3.
[82] C. Urués, G. Chopo-Escuin, J. Tommassen, R.C. Mainar-Jaime, J. Arenas, Biofilms as promoters of bacterial antibiotic resistance and tolerance, Antibiotics. (Basel) 10 (1) (2020) 3, https://doi.org/10.3390/antibiotics10010003.
[83] M.K. Luther, S. Bilida, L.A. Mermel, K.L. LaPlante, Ethanol and isopropyl alcohol exposure increases biofilm formation in staphylococcus aureus and staphylococcus epidermidis, Infect. Dis. Ther. 4 (2) (2015) 219–226, https://doi.org/10.1007/s40121-015-0065-y.
[84] G. McDonnell, A.D. Russell, Antiseptics and disinfectants: activity, action, and resistance, Clin. Microbiol. Rev. 12 (1) (1999) 147–179, https://doi.org/10.1128/CMR.12.1.147.
[85] R. Salvage, C.M. Hull, D.E. Kelly, S.L. Kelly, Use of 70 % alcohol for the routine removal of microbial hard surface bioburden in life science cleanrooms, Future Microbiol. 9 (10) (2014) 1123–1130, https://doi.org/10.2217/fmb.14.73.
[86] Y.W.S. Yeung, Y. Ma, S.Y. Liu, W.H. Pun, S.L. Chua, Prevalence of alcohol-tolerant and antibiotic-resistant bacterial pathogens on public hand sanitizer dispensers, J. Hospit. Infect. 127 (2022) 26–33, https://doi.org/10.1016/j.jhin.2022.05.017.
[87] P.R. More, S. Pandit, A.D. Filippis, G. Franci, I. Mijakovic, M. Galdiero, Silver nanoparticles: bactericidal and mechanistic approach against drug resistant pathogens, Microorganisms. 11 (2) (2023) 369, https://doi.org/10.3390/microorganisms11020369.
[88] S. Anees Ahmad, S. Sachi Das, A. Khatoon, M. Tahir Ansari, Mohd. Afzal, M. Saquib Hasnain, A. Kumar Nayak, Bactericidal activity of silver nanoparticles: a mechanistic review, Mater. Sci. Energy Technol. 3 (2020) 756–769, https://doi.org/10.1016/j.mset.2020.09.002.
[89] J. Xu, Q. Lin, M. Sheng, T. Ding, B. Li, Y. Gao, Y. Tan, Antibiofilm effect of cinnamaldehyde-chitosan nanoparticles against the biofilm of staphylococcus aureus, Antibiotics 11 (10) (2022) 1403, https://doi.org/10.3390/antibiotics11101403.
[90] H. Yilmaz Atay, Antibacterial activity of chitosan-based systems, in: S. Jana, S. Jana (Eds.), Functional Chitosan, Springer Singapore, Singapore, 2019, pp. 457–489, https://doi.org/10.1007/978-981-15-0263-7_15.
[91] W. Wahyuningsih, M. Miranti, H.Y. Teruna, T.T. Nugroho, Isolation of a high antioxidant non-toxic polar fraction from Garcinia mangostana fruit pericarp by reverse phase column chromatography, J. Kimia Sains dan Aplikasi 24 (1) (2021) 15–21, https://doi.org/10.14710/jksa.24.1.15-21.
[92] M. Chandrasekaran, K. Kim, S. Chun, Antibacterial activity of chitosan nanoparticles: a review, Processes 8 (9) (2020) 1173, https://doi.org/10.3390/pr8091173.